



Defence Research and
Development Canada

Recherche et développement
pour la défense Canada



Surface Plasmon Resonance Spectroscopy of Gold Nanoparticle- Coated Substrates

Use as an Indicator of Exposure to Chemical Warfare Simulants

D.B. Pedersen & E.J.S. Duncan
Defence R&D Canada – Suffield

Technical Report
DRDC Suffield TR 2005-109
August 2005

Canada

Surface Plasmon Resonance Spectroscopy of Gold Nanoparticle- Coated Substrates

Use as an Indicator of Exposure to Chemical Warfare Simulants

D. B. Pedersen & E. J. S. Duncan

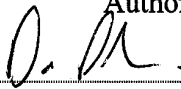
Defence R&D Canada – Suffield

Technical Report

DRDC Suffield TR 2005-109

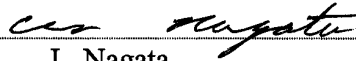
August 2005

Author



D. B. Pedersen, E. J. S. Duncan

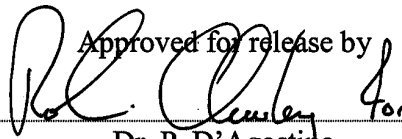
Approved by



L. Nagata

Head/ Chemical and Biological Defence Section

Approved for release by



Dr. P. D'Agostino

Chairman/ Document Review Panel

© Her Majesty the Queen as represented by the Minister of National Defence, 2005

© Sa majesté la reine, représentée par le ministre de la Défense nationale, 2005

Abstract

Gold nanoparticles with diameters of 9 ± 6 nm have been synthesized, using the citrate reduction method, and deposited onto quartz substrates. The responsiveness of the resulting gold nanoparticle films to gas-phase warfare agent simulant exposures has been examined using 2-chloroethyl ethyl sulfide and paraoxon. Significant shifts in the peak position of the surface plasmon resonance associated with the nanoparticles were observed in both cases. This shift was reversible and the peak positions returned to their pre-exposure values once the simulants were removed. The response to the exposure events was also found to be faster than ~ 10 s, the rate at which data was acquired in the experiments. A larger shift was observed upon exposure of the films to formaldehyde, a highly hazardous toxic industrial chemical. Unlike, 2-chloroethyl ethyl sulfide and paraoxon, the shift was not readily reversible and extensive heating and pumping under vacuum was required to shift the peak position back to pre-exposure values. Through analysis of the 2-chloroethyl ethyl sulfide and paraoxon data, ~ 600 pM and ~ 2 nM are estimated as lower detection limits for the two simulants, respectively.

Résumé

Des nanoparticules d'or ayant des diamètres de 9 ± 6 nm ont été synthétisées par une méthode de réduction de citrate et ont été déposées sur des substrats de quartz. La réactivité qui résulte des expositions des films de nanoparticules d'or au simulant d'un agent de guerre en phase gazeuse, a été examinée en utilisant le sulfure d'éthyle de 2-chloréthyle et le paraoxon. Des changements importants dans la position de crête de la détection par résonance plasmonique de surface associée aux nanoparticules ont été observés dans les deux cas. Le changement était réversible et les positions de crêtes ont repris leurs valeurs de pré-exposition une fois que les simulants ont été supprimés. On a aussi trouvé que la réponse aux cas d'exposition était plus rapide que ~ 10 s, le taux auquel les données ont été acquises durant les expériences. Un changement plus important a été observé lors de l'exposition des pellicules au formaldéhyde, un produit chimique industriel toxique très dangereux. Contrairement au sulfure d'éthyle de 2-chloréthyle et au paraoxon, le changement n'était pas facilement réversible et il a fallu un pompage et un chauffage sous vide prolongé pour obtenir de nouveau la position de crête au niveau des valeurs de pré-exposition. L'analyse des données permet d'estimer que les limites de détection ~ 600 pM et ~ 2 nM sont les plus faibles pour les deux simulants, le sulfure d'éthyle de 2-chloréthyle et le paraoxon, respectivement.

This page intentionally left blank.

Executive summary

Incorporation of nanoparticles into materials affords opportunities to impart functionality to the materials and provides an avenue towards next-generation protective materials. Surface plasmon resonance (SPR) spectroscopy is a sensitive technique that may be used to exploit the optical properties of metal nanoparticles and their sensitivity to modifications of their ambient medium for the purposes of improving the protection of the soldier in a threat environment. The technique requires little in the way of specialized equipment and can be performed with a standard ultraviolet-visible (UV-vis) spectrometer. Nonetheless, SPR spectroscopy routinely detects various analytes with extremely high sensitivity using standard absorption spectrometers. A strong broad SPR absorption band is observed in the absorption spectra of many metallic nanoparticles, in particular those of gold and silver. In addition to being size-dependent, the surface plasmon resonance band is also extremely sensitive to changes in the refractive index of the medium surrounding the particle. In this context, the nanoparticles have an inherent sensing ability. Any species adsorbed to the nanoparticle surface will manifest a colour change (shift in the SPR peak position) proportional to the magnitude of the change in the refractive index near the nanoparticle surface.

The work described in this report describes the synthesis of nanoparticles with properties appropriate for protection applications. The optical properties of the resulting gold nanoparticle films was demonstrated to be very consistent for numerous solvent systems and the responsiveness of the gold nanoparticle films to gas-phase warfare agent exposures have been examined using 2-chloroethyl ethyl sulfide as a simulant for sulphur mustard and paraoxon as a simulant for nerve agent. Significant shifts in the peak position of the surface plasmon resonance associated with the nanoparticles were observed in both cases. Through analysis of the 2-chloroethyl ethyl sulfide and paraoxon data, a lower detection limit for our gold nanoparticle film SPR method is estimated on par with typical gas chromatography methods. The gold nanoparticle films were also shown to respond to formaldehyde vapour, a highly hazardous toxic industrial chemical.

Nanoparticles offer a route towards materials that selectively respond to specific threats in various ways. Nanoparticles could, for example, function as built-in sensing elements able to signal exposure to toxic chemical or biological agents before their levels become harmful. The ability of certain materials such as alkali earth metal oxides in the form of particles or crystallites of nanometre dimensions to degrade warfare agents to non-toxic products has been previously demonstrated. The unique reactivity of these nanoparticles may be exploited to develop reactive, self-decontaminating materials. This initial work lays the foundation for subsequent studies where these nanoparticles will be utilized as built-in sensors, reactive components, or super-adsorbents in next-generation protective materials.

Pedersen, David B. and Duncan, E.J. Scott. 2005. Surface Plasmon Resonance Spectroscopy of Gold Nanoparticle-Coated Substrates: Use as an Indicator of Exposure to Chemical Warfare Simulants. DRDC Suffield TR 2005-109. Defence R&D Canada – Suffield.

Sommaire

L'incorporation de nanoparticules dans les matériaux offre l'opportunité de conférer de la fonctionnalité dans les matériaux et ouvre la voie à une génération future de matériaux de protection. La spectroscopie de détection par résonance plasmonique de surface est une technique sensible pouvant être utilisée pour exploiter les propriétés optiques de nanoparticules de métal ainsi que leur sensibilité aux modifications de leur médium ambiant, ceci dans le but d'améliorer la protection du soldat situé en milieu dangereux. La technique requiert peu d'équipement spécialisé et peut être effectuée avec un appareil standard de spectrométrie ultraviolette et visible. La spectroscopie de détection par résonance plasmonique de surface n'en détecte pas moins des mélanges à analyser variés, automatiquement et avec une extrême sensibilité, en utilisant des spectromètres d'absorption standard. On a observé une large bande efficace d'absorption de détection par résonance plasmonique de surface dans le spectre d'absorption de beaucoup de nanoparticules métalliques, en particulier celles qui sont d'or ou d'argent. La bande de détection par résonance plasmonique de surface non seulement dépend de la taille mais est extrêmement sensible aux changements de l'index de réfraction du médium qui entoure la particule. Dans ce contexte, les nanoparticules ont une capacité inhérente de détection. Toutes espèces adsorbées par la surface de nanoparticules changeront de couleur (correspondant à un changement dans la position de crête de la détection par résonance plasmonique de surface) proportionnellement à la magnitude du changement dans l'index de réfraction proche de la surface des nanoparticules.

Le travail, dans ce rapport, décrit la synthèse des nanoparticules ayant des propriétés appropriées aux applications reliées à la protection. On a démontré que les propriétés optiques des pellicules de nanoparticules d'or qui en résultent sont très compatibles avec de nombreux systèmes de solvants. De plus, la réactivité des pellicules de nanoparticules d'or aux expositions d'agents de guerre en phase gazeuse ont été examinées en utilisant le sulfure d'éthyle de 2-chloréthyle comme simulant pour le gaz moutarde, et le paraoxon comme simulant pour les agents neurotoxiques. On a observé des changements importants dans la position de crête de la détection par résonance plasmonique de surface associés au nanoparticules. L'analyse des données du sulfure d'éthyle de 2-chloréthyle et du paraoxon a permis d'estimer que la limite de détection la plus basse pour la méthode de détection par résonance plasmonique de surface avec le filme de nanoparticules d'or est comparable à celle des méthodes de chromatographie en phase gazeuse ordinaires. On a aussi montré que les pellicules de nanoparticules d'or réagissent à la vapeur de formaldéhyde, un produit chimique industriel toxique très dangereux.

Les nanoparticules ouvrent la voie à la création de matériaux qui répondraient à des menaces spécifiques, sélectivement et de manières différentes. Les nanoparticules pourraient, par exemple, fonctionner comme des éléments de détection intégrés, capables de signaler l'exposition à des agents chimiques ou biologiques toxiques avant que les niveaux deviennent dangereux. On a démontré antérieurement que certains matériaux, tels que les métaux terreux alcalins, sous forme de particules ou de cristallite de dimension nanométrique, ont la capacité de dégrader les agents de guerre en produits non toxiques. La réactivité particulière de ces nanoparticules peut être exploitée pour développer des matériaux réactifs, auto-décontaminants. Ces travaux initiaux posent les jalons pour des études ultérieures où ces nanoparticules seront utilisées comme détecteurs intégrés, composants réactifs ou super-adsorbants de la génération future des matériaux de protection.

Pedersen, David B. and Duncan, E.J. Scott. 2005. Surface Plasmon Resonance Spectroscopy of Gold Nanoparticle-Coated Substrates: Use as an Indicator of Exposure to Chemical Warfare Simulants. DRDC Suffield TR 2005-109. R & D pour la défense Canada – Suffield.

Table of contents

Abstract.....	i
Résumé	i
Executive summary	iii
Sommaire.....	iv
Table of contents	v
List of figures	vi
List of tables	vii
Introduction	1
Method.....	4
Chemicals	4
Materials	4
Equipment.....	4
Preparation of Gold Nanoparticles in Solution.....	4
Preparation of Gold Nanoparticle Films on Quartz Substrates	5
Surface Plasmon Resonance Calibration for Gold Nanoparticle Films.....	5
Response of Gold Nanoparticle Films to Vapour Exposure.....	7
Results	9
Discussion.....	19
Summary and Conclusions	25
Annexes	26
List of symbols/abbreviations/acronyms/initialisms	29
References	30

List of figures

- Figure 1: Gas cell connected in-line with the UV-vis spectrometer. The blue cables are the optic fibres connected to the Ocean Optics spectrometer. The cell is wrapped in heating tape for temperature control although this feature was not utilized in this work. Two Teflon gas-handling lines exit out of the top of the cell: one equipped with a toggle valve and the other with a needle valve. The gas cylinder attached to the aluminum post was not used for these experiments. For clarity, the gas bulb and water bath have been removed so that the cell can be seen. 8
- Figure 2: Absorption spectrum measured for a “cherry red” gold nanoparticle solution. The black overlay curve is a mathematical fit of Eq. 1 to the data between $510 < \lambda < 575$ nm and used to determine the wavelength corresponding to the peak of the surface plasmon resonance ($\lambda_{\text{peak}} = 517.87$ nm). a.u. denotes absorbance units. 9
- Figure 3: Absorption spectra in the SPR region of various sized nanoparticles synthesized via sequential deposition of layers of Au onto CR nanoparticles. The sizes of the nanoparticles with peaks at 520, 543, and 558 nm were determined via comparison with literature data and found to be 14, 74, and 86 nm in diameter, respectively.³⁵ See text for details. 10
- Figure 4: Preliminary STM data of some nanoparticles on a gold surface are shown on the left. The sample was prepared by drying a drop of cherry red solution on a gold substrate. Just right of centre, appear to be two oval-shaped nanoparticles in contact with each other. On the right, a cross section of one of the nanoparticles is shown. The overall length of the nanoparticle is ~ 20 nm. This dimension is known to be inaccurate, however, because the STM tip has a finite width.³⁶ The height of the particle is ~ 2.5 nm. The height is known to be a more accurate measure of the particle diameter. 11
- Figure 5: Absorption spectrum of the surface plasmon resonance measured for a gold nanoparticle-coated quartz substrate made from “cherry red” gold nanoparticle solution. The black overlay curve is a mathematical fit of Eq. 1 to the data between $510 < \lambda < 575$ nm and used to determine the wavelength corresponding to the peak of the surface plasmon resonance ($\lambda_{\text{peak}} = 523.59$ nm). 12
- Figure 6: Response functions of gold nanoparticle films immersed in four different liquid solvents. The different data sets correspond to replicate gold films that are different due to variability in the deposition process. The solvents used, in order of refractive index, are acetone, n-heptane, dichloromethane and toluene. 13
- Figure 7: The response functions of gold nanoparticle films determined using an ethanol/toluene binary solvent series. Data for four different gold films are shown. (NOTE: assumes that the refractive index of the mixtures is the composition-weighted average of the refractive indices of toluene and ethanol) 14

Figure 8: SPR peak position vs. time for an experiment where a gold nanoparticle film was exposed to 2-chloroethyl ethyl sulfide vapour. Each step up in wavelength corresponds to an injection of vapour into the gas cell containing the nanoparticle film. Each step down corresponds to evacuation of the cell. The SPR peak position at each time (10 s) was determined by fitting Eq 1 to the SPR absorbance spectrum. See text for details. . 15

Figure 9: SPR peak position vs. time for an experiment where a gold nanoparticle film was exposed to 2-chloroethyl ethyl sulfide vapour is shown in the upper graph. Each step up in wavelength corresponds to an injection of vapour into the gas cell containing the nanoparticle film. Each step down corresponds to evacuation of the cell. The SPR peak position at each time (10 s) was determined by fitting Eq 1 to the SPR absorbance spectrum. The broken line is a guide to the eye to help show the reproducibility of the step size. Both cell and bath were at room temperature. The lower graph is a plot of the step size, on the right side of each step (i.e. after an equilibration period), determined for each measurement. See text for details. 16

Figure 10: SPR peak position vs. time for an experiment where a gold nanoparticle film was exposed to paraoxon vapour. Each step up in wavelength corresponds to an injection of vapour into the gas cell containing the nanoparticle film. Each step down corresponds to evacuation of the cell. The SPR peak position at each time (10 s) was determined by fitting Eq 1 to the SPR absorbance spectrum. See text for details 17

Figure 11: Plot of SPR peak position vs. time collected when a gold nanoparticle film was exposed to formaldehyde. The times corresponding to injection, evacuation, and heating of the gas cell are labelled. 18

Figure 12: A section of the data shown in Fig. 6 corresponding to the highest temperature, and therefore highest 2-chloroethyl ethyl sulfide pressure, employed. The solid line is a fit of the equation shown to the data..... 22

Figure 13: Plot of the change in SPR peak position ($\Delta\lambda$) observed upon exposure of a gold nanoparticle film to 2-chloroethyl ethyl sulfide versus concentration of the sulfide. The solid line is presented as a guide to the eye of the trend in the data. 23

List of tables

Table 1: Bulk refractive index of 4 different mediums used to generate the surface plasmon resonance versus refractive index plots for the gold nanoparticle films developed in this study. 6

Table 2: Fraction of ethanol and toluene in five binary mixtures of ethanol and toluene and corresponding bulk refractive index. (NOTE: assumes that the refractive index of the mixtures is the composition-weighted average of the refractive indices of toluene and ethanol)..... 6

This page intentionally left blank.

Introduction

Surface plasmon resonance (SPR) spectroscopy is a sensitive technique in which the optical properties of metal nanoparticles and their sensitivity to modifications of their ambient medium are exploited. The technique requires little in the way of specialized equipment and can be performed with a standard ultraviolet-visible (UV-vis) spectrometer. Nonetheless, SPR spectroscopy routinely detects various analytes with picomolar sensitivity using standard absorption spectrometers. Using more elaborate optical detection approaches, zeptomolar (10^{-21} M) sensitivity can be achieved.[1] In light of the high sensitivity and relatively simple experimental apparatus required, SPR spectroscopy is evolving to become a standard analytical technique. In typical analytical applications, gold (Au) or silver (Ag) nanoparticles are utilized because they are not overly reactive, i.e. they are stable, and because they are visibly coloured, which conveniently allows use of standard ultraviolet-visible (UV-vis) equipment. Most often, these particles are coated (functionalized) with molecules tailor-synthesized so that they bind to target molecules of interest. These coatings are often biomolecule receptors such as proteins or DNA strands that bind specifically to target molecules such as substrates or complementary DNA strands.[2,3] In all cases, the working premise of SPR spectroscopy is that adsorption of the target to the nanoparticle or nanoparticle-bound receptor manifests a change in the colour (optical absorbance) of the nanoparticle. This change may be detected optically signalling the presence of the target molecule. A tremendous amount of work has been done to develop SPR spectroscopy as a sensor technology and over 1000 papers were published in 2004.

A strong broad absorption band is observed in the absorption spectra of many metallic nanoparticles, in particular those of gold and silver. This occurs because of the coupling of incident electromagnetic radiation into a surface plasmon (described as a collective oscillation of the conduction electrons) at the interface between the particle and the medium surrounding the particle.[4,5] The resulting energy loss is manifested as an absorbance known as the surface plasmon band. Many of the distinctive colours of nanoparticle colloids of noble, alkali, alkaline earth and rare earth metals may be attributed to the presence of this surface plasmon absorption band.[6] Being confined to the surface, this collective oscillation of the free electrons is sensitive to changes in the size of the particle and as the diameter gets smaller the energy required to collectively excite motion of the surface plasmon electrons increases.[7] For Au nanoparticles with diameters near 5 nm, for example, the energy required to excite the surface plasmon is comparable to the energy of visible light. Thus, the particles strongly absorb at visible wavelengths with a maximum absorbance near 520 nm. Au nanoparticles with diameters larger than 5 nm have maxima at longer wavelengths and by varying the particle size one can tune the maximum of the SPR absorbance to be anywhere from 520 nm to beyond 1000 nm (i.e. right from the visible into the near-infrared). In addition to being size-dependent, the surface plasmon resonance band is also extremely sensitive to changes in the dielectric properties of the surrounding medium.[8] Media of high dielectric constants (refractive indices) are effectively more polarizable and thus couple with the surface plasmon electrons more readily and the energy required to collectively excite the electrons is decreased. That is, the maximum in the SPR absorbance shifts to lower energy (longer wavelengths). In this context, the nanoparticles have an inherent sensing ability. Any species adsorbed to the nanoparticle surface will manifest a colour change (shift in the SPR peak position) proportional to the magnitude of the change in the refractive index near the nanoparticle surface. Only changes near the nanoparticle surface are sensed as the SPR is only

sensitive to the medium within roughly one wavelength distance from the surface.[9] For visible light, only changes in refractive index occurring at distances within ~200 nm of the particle surface cause changes in the optical properties of the nanoparticles.[5,10, 11] Thus, the nanoparticles are most sensitive to adsorption directly to the particle surface.

With increases in the refractive index of the medium, SPR peak positions shift in a well-behaved manner to longer wavelengths. For nanoparticles of fixed size, a plot of the SPR peak position versus refractive index of the surrounding medium is often a straight line. Such plots are common in SPR spectroscopy literature and are called response functions. They have been characterized in terms of a responsiveness equation[5]

$$\Delta\lambda_{\text{peak}} = m\eta \quad \text{Eq. (1)}$$

where $\Delta\lambda_{\text{peak}}$ is the shift in the SPR peak position, η is the refractive index of the medium, and m is the responsiveness of the nanoparticle. High responsiveness indicates a relatively large shift in wavelength upon change in medium refractive index. This would be a very desirable property for a SPR-based sensor platform. As the responsiveness is very sensitive to nanoparticle size and nanoparticle preparation, the responsiveness curves can also be used as a way of comparing the consistency of various nanoparticle preparation methods.

Recent work in nanoparticle-based sensors has seen progress in several directions. Target-molecule-induced aggregation of nanoparticles has been shown to be an effective DNA sensor. SPR-based detection of specific DNA sequences has been shown to be about two orders of magnitude more sensitive than the fluorescence techniques more commonly used.[12,13,14,15,16,17] This approach relies on detecting changes in the optical properties of gold nanoparticles caused by DNA-induced aggregation of the nanoparticles. Briefly, two types of nanoparticles are synthesized: half of the particles are functionalized with thiol-terminated single-stranded DNA with a base sequence complementary to one end of the target molecule; the other half are similarly functionalized but with a base sequence complementary to the other end of the target molecule. The thiol binds to the gold. When the target DNA is encountered, one end of the target binds to the DNA on the first type of functionalized nanoparticle and the other end binds to nanoparticles of the second type. In this way, the nanoparticles aggregate under the binding influence of the target DNA. This aggregation manifests a significant change in the dielectric properties of the medium surrounding the nanoparticles and a colour change is detected.[18,19]

Functionalization of nanoparticles with target-specific acceptors is perhaps the most active area of nanoparticle-based sensor research.[20,21] These efforts aim to exploit the selective affinity of biomolecules, typically, for specific targets. For example, Ag nanoparticles deposited on quartz substrates were recently functionalized with biotin.[22] Biotin has a high affinity for streptavidin with which it binds strongly and selectively. The biotin-functionalized nanoparticles therefore function as streptavidin-specific optical sensors. Exposure of the functionalized nanoparticles to 100 nM streptavidin solution shifts the maximum of the SPR absorption 27.0 nm to longer wavelengths—a shift that is easily detected. This simple example clearly illustrates how target-specific nanoparticle sensors can be made and utilized. In reality, however, nanoparticle-based detection schemes can be much more complicated, particularly when surface-enhancement effects are utilized to increase sensitivity. Metal nanoparticle-based sensors are inherently conducive to surface-enhanced spectroscopy,[23] which affords sensitivities high enough to make single-particle detection possible.[24,25,26]

Nanoparticle synthesis has a long history and nanoparticles have been utilized for colouring stained glass and clays for hundreds of years or more. At present, the most common synthesis method is the reduction of metal salts using citrates, as established by Turkevich.[27,28,29] Using the Turkevich method, the size of the nanoparticles generated can be controlled by varying the concentrations of the metal salt and the citrate reducing agent. As particle size increases, however, aggregation and precipitation eventually occur which places an upper limit on the size of nanoparticles that can be conveniently synthesized using this approach. To synthesize larger particles, surfactants must be added. These adhere to the nanoparticle surface thus preventing nanoparticle coalescence. Varying surfactant concentration also gives some control over the size of particles produced. Relatively high concentrations impede particle coalescence and growth processes and smaller particles result. Alternative approaches to nanoparticle synthesis such as nano-sphere lithography[30,31] have also been demonstrated, but are not relevant to the work discussed below.

Incorporation of nanoparticles into materials affords opportunities to impart functionality to the materials and provides an avenue towards next-generation protective materials and material systems. Nanoparticles could, for example, function as built in sensing elements able to signal exposure to toxic chemical or biological agents before their levels become harmful. Nanoparticles functionalized with biotin, for example, have been used to detect streptavidin at concentrations less than 700 pM.[22] Nanoparticles functionalised with organophosphorous hydrolase are another example of target-specific acceptors. These have been used to detect paraoxon, which simulates the properties of some nerve agents, with a detection limit of 10^{-8} M.[32] The unique reactivity of nanoparticles can also be exploited to develop reactive, self-decontaminating materials. The ability of nanoparticles to degrade warfare agents to non-toxic products has been demonstrated.[33,34] In short, nanoparticles offer a route towards materials that selectively respond to specific threats in various ways. Along this vein, this report summarizes our efforts to semi-quantitatively test the feasibility of sensing chemical warfare agent simulants with nanoparticles using the SPR approach. Citrate reduction of metal salts is employed and the synthesis methods are described. We also describe how these nanoparticles were deposited onto glass substrates using a silanization procedure. The optical properties of the resulting gold nanoparticle films are then described and their inherent sensing abilities demonstrated. Specifically, we examine the suitability of the SPR approach for detection of 2-chloroethyl ethyl sulfide and paraoxon, both chemical warfare agent simulants, as well as formaldehyde, a highly toxic industrial chemical.

Method

Chemicals

The following chemicals and solvents were purchased from Aldrich and used as received: 3-aminopropyltriethoxy-silane (99%), hydrogen tetrachloroaurate(III) trihydrate (17 wt % solution in dilute HCl), sodium citrate dihydrate (99%), 2-chloroethyl ethyl sulphide (98%), paraoxon (diethyl p-nitrophenyl phosphate), as well as research grade acetone, ethanol, n-heptane, dichloromethane, and toluene.

Materials

Fisher finest Premium microscope slides, (3" × 1" × 1 mm) from Fisher Scientific, were used as quartz substrates for the nanoparticle films.

Equipment

Ocean Optics SD2000 spectrometer equipped with UV-resistant optic fibre extensions and a halogen/deuterium DH2000 light source. For this work, only the halogen source was used.

Nanosurf EasyScan scanning tunnelling microscope.

Preparation of Gold Nanoparticles in Solution

A 2.0 mM stock solution of hydrogen tetrachloroaurate(III) (HAuCl_4) was prepared by adding 200 μL of the gold chloride salt solution to 100 mL distilled water. The reducing agent (2.0 mM solution of sodium citrate) was prepared by adding 30 mg sodium citrate dihydrate to 50 mL of distilled water. Initially the reduction of the gold chloride salt was carried out in a 50 mL beaker using the following components: 9.75 mL of distilled water, 0.25 mL of stock gold chloride solution and 10 mL of reducing agent stock solution. This procedure was also scaled-up by a factor of 10 without any problems. Following mixing, the beaker containing the gold chloride salt and reducing agent was placed on a stirring hotplate pre-set to heat the solution to 75 °C at a gentle stir. Within 10 to 20 min the colour of the solution changed from clear to mauve. Further heating caused the solution to become more red in colour. To monitor the progression of the synthesis, at this time samples of the solution (2-3 mL) can be removed from the beaker every few minutes, transferred to a cuvette and the optical spectrum measured to determine the wavelength of the surface plasmon resonance peak. Typically the first sample taken after the solution begins to take on a red colouration has a surface plasmon peak at ~ 525 nm. Heating/stirring is continued until no further change is observed in the wavelength of the surface plasmon resonance peak. The final maximum absorbance peak varies between 518 – 520 nm and may require 30 – 40 min cumulative heating. The colour of the solution at this time is described as “cherry red” (CR). The final solutions are stable for months or more with no measurable colour change or shift in surface plasmon resonance.

Larger nanoparticles were made by using the CR particles as seeds onto which additional gold was deposited. For example, 3 mL of CR solution was mixed with 10 mL of stock gold solution and 10 mL of citrate solution. This mixture was left to sit for 30-45 min after which the colour of the solution had changed, becoming more purple-blue. The change in colour is symptomatic of an increase in particle size due to the reduction of gold directly onto the seed (CR) nanoparticle surfaces. For even larger particles 3 mL of this purple-blue solution was then mixed with 10 mL of stock gold solution and 10 mL of citrate solution. After 30-45 min this solution became even more blue in colour indicative of the formation of even larger nanoparticles. Such sequential reduction of gold onto seed particles allowed for synthesis of particles of varying size, as indicated by their colour.

Preparation of Gold Nanoparticle Films on Quartz Substrates

The quartz substrates for the gold nanoparticle films were first functionalised with 3-aminopropyltriethoxy-silane to improve the adhesion of the gold nanoparticles to the quartz. This silanization process was found necessary to obtain a consistently high deposition and homogeneous coverage of the gold nanoparticles on the quartz. The procedure is as follows: 1) the quartz slides were soaked in acetone for 2 min and then rinsed thoroughly twice with distilled water; 2) the slides were then soaked in a 9:1 solution of distilled water and amino-silane for 5 min followed by a thorough rinsing with distilled water; 3) the final step was curing in an oven at 80 °C for 30 min. Functionalised slides were stored in a sealed container with desiccant.

In a 50 mL beaker 5.5 mL of the 2.0 mM gold stock solution was added to 4.5 mL of the CR gold nanoparticle solution. A silanized quartz slide was placed vertically into the mixture and held in position with laboratory parafilm such that it was free from touching the sides of the beaker. The quartz substrate was left to soak in the gold-salt/gold nanoparticle solution for 8 h. This time was determined adequate to coat the substrate with a sufficient density of gold nanoparticles to obtain a strong absorbance spectrum with the UV/vis spectrometer but maintain near-monolayer coverage and minimal aggregation of the nanoparticles. Immediately on removing the gold nanoparticle-coated quartz substrate from the mixture it was rinsed in a beaker containing acetone for approximately 5 s. Following this the gold-coated slides were placed in an oven at 200 °C for 60 min.

Surface Plasmon Resonance Calibration for Gold Nanoparticle Films

SPR response curves were determined using two different approaches. In the first method, the SPR of the gold nanoparticle film was measured on immersion of the film in four different organic solvents each with a distinct refractive index. Table 1 lists the various solvents and their refractive indices. Specifically, quartz slides coated with gold nanoparticles were cut to a size that would fit into a quartz cuvette for use with the UV-vis spectrometer. The SPR response (absorbance spectrum) of the gold nanoparticle film for each organic solvent was measured in turn commencing either with the solvent having the highest or lowest refractive index. Following each measurement the gold nanoparticle film was removed from the cuvette and soaked and rinsed in a beaker containing the next solvent in the series before acquiring a new measurement in that solvent. Reference (baseline) measurements were obtained for each solvent using a blank quartz substrate.

Table 1: Bulk refractive index of 4 different mediums used to generate the surface plasmon resonance versus refractive index plots for the gold nanoparticle films developed in this study.

Medium	Bulk Refractive Index
Toluene	1.493
Dichloromethane	1.421
n-heptane	1.387
Acetone	1.355

In the second method, the SPR response of the gold nanoparticle film was measured on immersion in five binary mixtures of various concentrations of two highly miscible organic solvents, toluene and ethanol, as given in Table 2. The SPR response was measured for neat toluene and ethanol as well. The SPR response of the gold nanoparticle film for each mixture in the ethanol/toluene series was measured commencing with neat toluene. Following each measurement the gold nanoparticle film was removed from the cuvette while a new reference (baseline) measurement was acquired with a blank quartz substrate immersed in the next mixture.

Table 2: Fraction of ethanol and toluene in five binary mixtures of ethanol and toluene and corresponding bulk refractive index. (NOTE: assumes that the refractive index of the mixtures is the composition-weighted average of the refractive indices of toluene and ethanol)

Fraction of ethanol (%)	Fraction of toluene (%)	Binary mixture refractive index
100	0	1.363
83	17	1.385
67	33	1.406
50	50	1.428
33	67	1.450
17	83	1.471
0	100	1.493

Response of Gold Nanoparticle Films to Vapour Exposure

A gas cell was connected in-line with the Ocean Optics spectrometer as shown in Figure 1. The stainless steel gas cell has a volume of 125 mL and is equipped with two quartz windows sealed to the cell with o-rings. The gas cell was fitted with two gas-handling lines: the first line was connected to a 131 mL glass bulb; the second line was connected to vacuum and pressurized He via a gas-handling manifold. Three chemical vapours were investigated; 2-chloroethyl ethyl sulphide, paraoxon and paraformaldehyde. For the first experiments with 2-chloroethyl ethyl sulphide, 50 - 100 μL was placed in the glass bulb that was then sealed and allowed to equilibrate at ambient temperature (23 $^{\circ}\text{C}$). 50 - 100 μL is sufficient to ensure that a saturated vapour state is readily achieved inside the glass bulb in a short period of time. After acquiring a reference spectrum with a blank quartz substrate, a gold nanoparticle film was placed in a clip holder and positioned in the gas cell. During this process a flow of He was maintained through the cell so as to prevent contamination with atmospheric water. The cell was then closed and placed under vacuum ($\sim 10^{-2}$ Torr). Full spectra, collected every ~ 10 s (integrated over 70 - 100 ms and averaged 100 times), were saved to file by the spectrometer. After 60 min of pumping on the cell and allowing the gas bulb to equilibrate, the cell was isolated from vacuum and the valve separating the gas cell and the gas bulb was opened thus transferring vapour from the bulb to the cell. The cell was then allowed to equilibrate for some minutes. Higher vapour pressures were attained by warming the glass bulb to 35 and 53 $^{\circ}\text{C}$ in a water bath. At these temperatures the bulb was open to the atmosphere so as to prevent a pressure build-up. After each experiment the cell was placed under vacuum for at least one hour so as to ensure no residual vapours remained in the cell. Several experiments were also completed using a known volume of 2-chloroethyl ethyl sulphide to generate a specific vapour pressure and molar concentration inside the gas cell at a specific temperature.



Figure 1: Gas cell connected in-line with the UV-vis spectrometer. The blue cables are the optic fibres connected to the Ocean Optics spectrometer. The cell is wrapped in heating tape for temperature control although this feature was not utilized in this work. Two Teflon gas-handling lines exit out of the top of the cell: one equipped with a toggle valve and the other with a needle valve. The gas cylinder attached to the aluminum post was not used for these experiments. For clarity, the gas bulb and water bath have been removed so that the cell can be seen.

A similar series of experiments were carried out using paraoxon and formaldehyde. In the case of paraoxon, 25 μL was placed in the glass bulb that was then heated for 60 min in a water bath to 54 and 73 $^{\circ}\text{C}$ to produce a saturated vapour state at these temperatures. To generate formaldehyde vapour, ~ 100 mg of paraformaldehyde was placed in the glass bulb and heated for 60 min to 50 $^{\circ}\text{C}$ so that decomposition occurred and formaldehyde was released.

Results

The surface plasmon resonance for a typical CR gold nanoparticle solution made according to the method described above is shown in Figure 2. The data are presented in terms of absorbance units (*a.u.*) versus wavelength (λ). As seen, a broad absorbance at visible wavelengths is observed corresponding to the optical excitation of the SPR of the nanoparticles. The wavelength corresponding to the peak of the surface plasmon resonance λ_{peak} was determined to be 517.87 nm. This value was obtained by curve-fitting the mathematical function

$$a.u. = A_1 + A_2 * \exp(-0.5 * (|\lambda - A_3| / A_4)^{A_5}) \quad \text{Eq. (2)}$$

to the spectral response between $510 < \lambda < 575$. Constants A_1 through A_5 are fitting parameters determined by non-linear regression. The function has the characteristic that $A_3 = \lambda_{\text{peak}}$ of the data used for the fit.

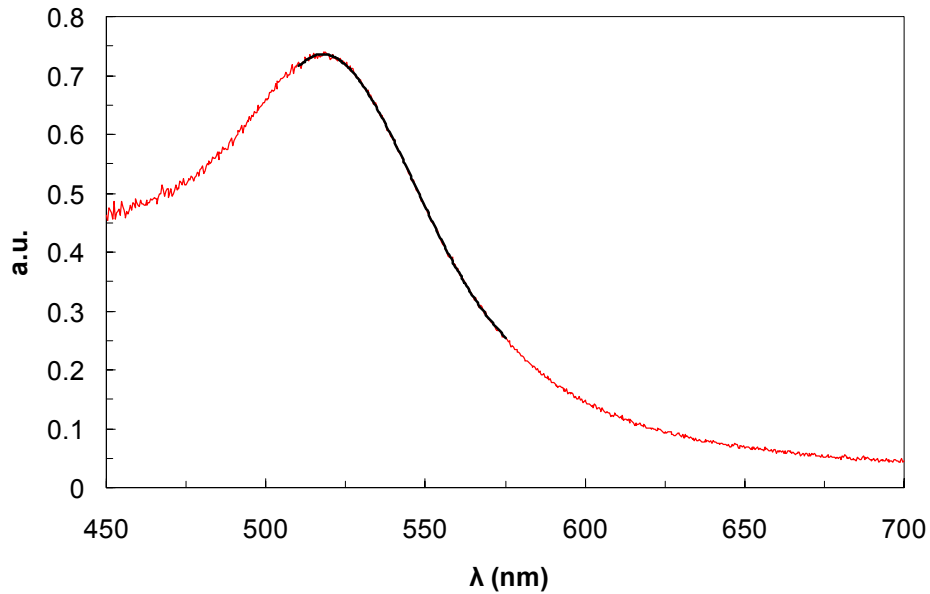


Figure 2: Absorption spectrum measured for a “cherry red” gold nanoparticle solution. The black overlay curve is a mathematical fit of Eq. 1 to the data between $510 < \lambda < 575$ nm and used to determine the wavelength corresponding to the peak of the surface plasmon resonance ($\lambda_{\text{peak}} = 517.87$ nm). *a.u.* denotes absorbance units.

Reduction of gold onto the surfaces of the CR nanoparticles resulted in formation of larger particles, as described above. Spectra for various sized nanoparticles synthesized through sequential deposition of layers of Au onto CR nanoparticles are shown in Figure 3. The SPR peak position shifts to increasingly longer wavelengths as the particle size increases, as expected. Comparing with literature values, the diameters of the nanoparticles in Figure 3 are 14, 74, and 86 nm.[35] Preliminary scanning tunnelling microscope (STM) images support these conclusions. STM images of the smallest nanoparticles (cherry red) were attained by drying a drop of solution on a gold substrate. A sample image is shown in Figure 4 along with a cross section of one of the particles. From the cross section, the height of the nanoparticle is ~ 3 nm and the length is ~ 20 nm. The former is a more accurate dimension as the latter is known to be distorted because of the finite width of the STM tip.[36,37] From literature, a 3 nm diameter particle would have a SPR peak near 520 nm, compatible with the results presented in Figure 2 and Figure 3. In consideration of both STM and absorbance data, the cherry red particles therefore have diameters between 3 and 14 nm (i.e. $\sim 9 \pm 6$ nm).

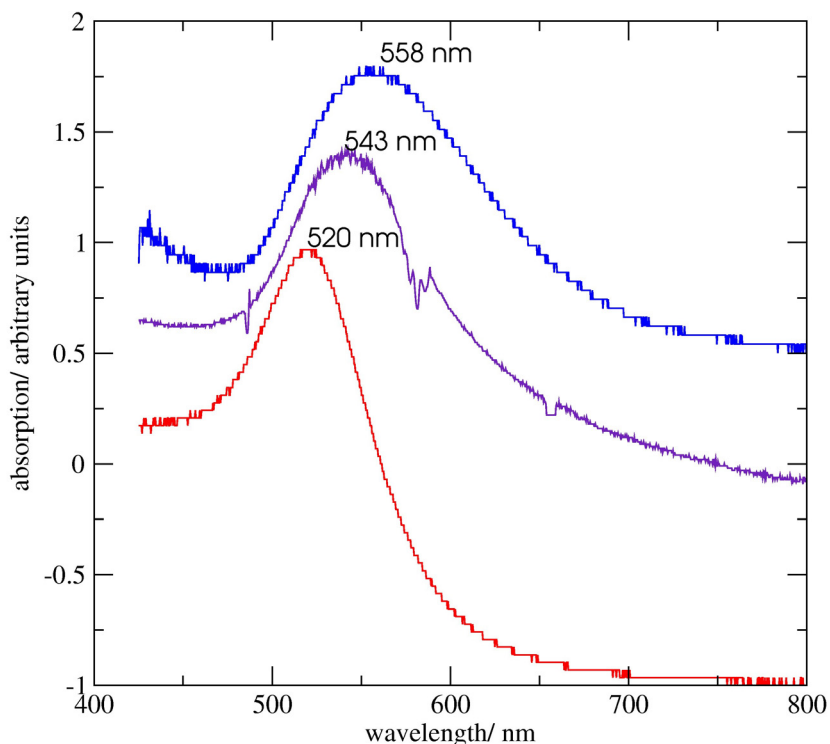


Figure 3: Absorption spectra in the SPR region of various sized nanoparticles synthesized via sequential deposition of layers of Au onto CR nanoparticles. The sizes of the nanoparticles with peaks at 520, 543, and 558 nm were determined via comparison with literature data and found to be 14, 74, and 86 nm in diameter, respectively. See text for details.

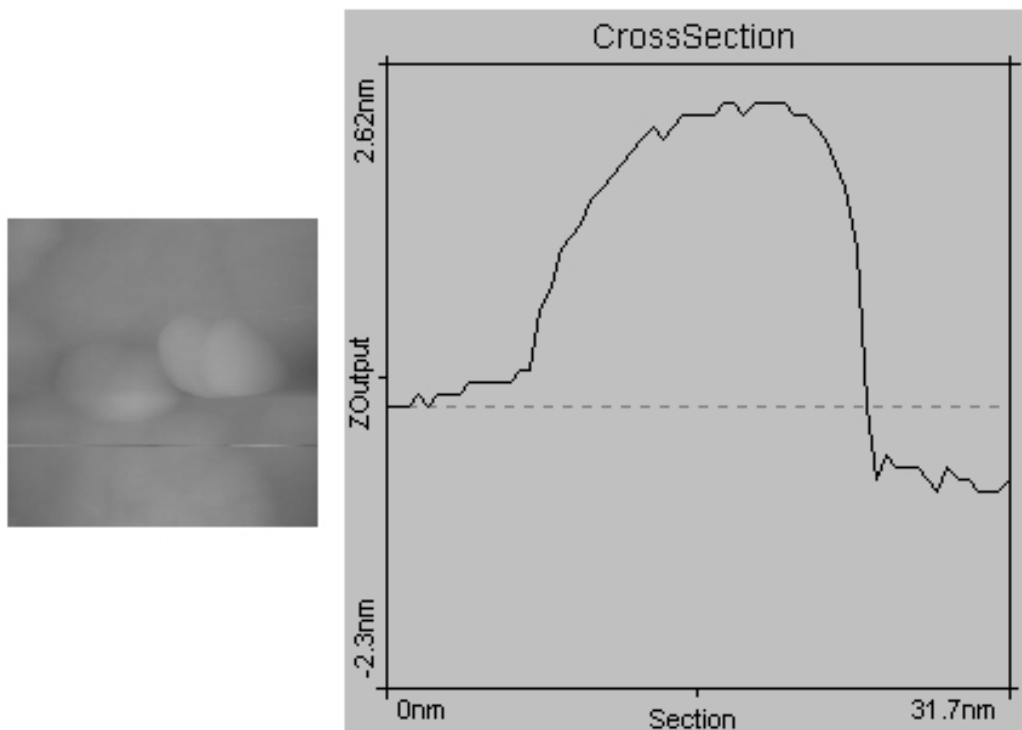


Figure 4: Preliminary STM data of some nanoparticles on a gold surface are shown on the left. The sample was prepared by drying a drop of cherry red solution on a gold substrate. Just right of centre, appear to be two oval-shaped nanoparticles in contact with each other. On the right, a cross section of one of the nanoparticles is shown. The overall length of the nanoparticle is ~20 nm. This dimension is known to be inaccurate, however, because the STM tip has a finite width.[36] The height of the particle is ~2.5 nm. The height is known to be a more accurate measure of the particle diameter.

Deposition of the gold nanoparticles onto functionalised quartz substrates manifested a shift in the SPR peak position. The spectrum of the surface plasmon resonance for a gold nanoparticle-coated quartz substrate made according to the method described above is shown in Figure 5. λ_{peak} was determined to be 523.59 nm using Eq. 1. This value is shifted from the $\lambda_{\text{peak}} = 517.87$ nm value obtained above for the nanoparticles in aqueous solution. The shift reflects the difference in the nature of the medium surrounding the nanoparticles in solution as compared to deposited on quartz.

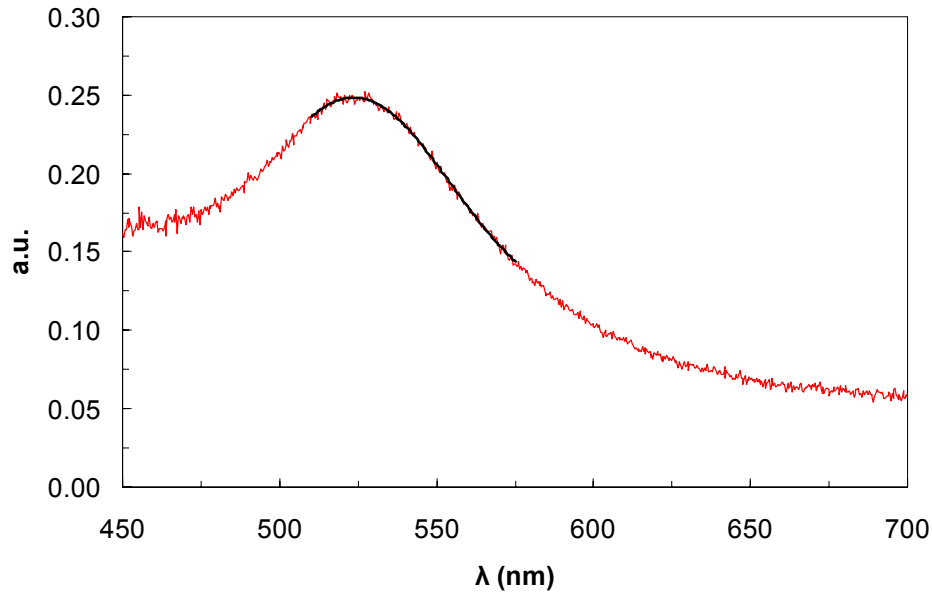


Figure 5: Absorption spectrum of the surface plasmon resonance measured for a gold nanoparticle-coated quartz substrate made from “cherry red” gold nanoparticle solution. The black overlay curve is a mathematical fit of Eq. 1 to the data between $510 < \lambda < 575$ nm and used to determine the wavelength corresponding to the peak of the surface plasmon resonance ($\lambda_{peak} = 523.59$ nm).

In Figure 6, response functions (λ_{peak} vs. refractive index) of the gold nanoparticle films are shown. Data for eight series of experiments are shown, each using a different gold nanoparticle-coated quartz substrate. The films are different, and have offset λ_{peak} values, due to variability in the nanoparticle-onto-quartz deposition process. Refer to Table 1 for the various solvents and their bulk refractive indices. As seen, the response is linear over the range of refractive index from toluene (1.493) to acetone (1.355) and may be represented very simply as

$$\lambda_{peak} = m\eta_{bulk} \quad \text{Eq. (3)}$$

where λ_{peak} is the wavelength corresponding to the peak of the surface plasmon resonance, m is the slope (also called the responsiveness) and η_{bulk} is the bulk refractive index of the material in contact with the surface of the gold. The mean and standard error of the slope m for a total of eight measurements was 57.53 ± 1.62 . A similar plot was generated using an ethanol/toluene binary solvent series as presented in Figure 7. As in Figure 6, the SPR peak position of the nanoparticle film immersed in binary mixtures of the two miscible solvents, toluene (1.493) and ethanol (1.363), is seen to be a linear function of the refractive index. The slope m of this plot was determined to be 61.26 ± 3.9 (std error), in agreement with the previous result of 57.53 ± 1.62 (see above) for the SPR calibration response shown in Figure 6. Statistically, the difference in the mean response values determined for the four solvents and that of the binary solvent mixture is not great enough to exclude the possibility that the difference is due to random sampling variability; there is not a statistically significant difference ($P = 0.313$). Differences in the slopes for both Figures 6 and 7 can be attributed to slight differences in the cleanliness of the nanoparticles, as a result of exposure to air-borne contaminants, or to variability in the process used to deposit the nanoparticles onto the quartz substrates.

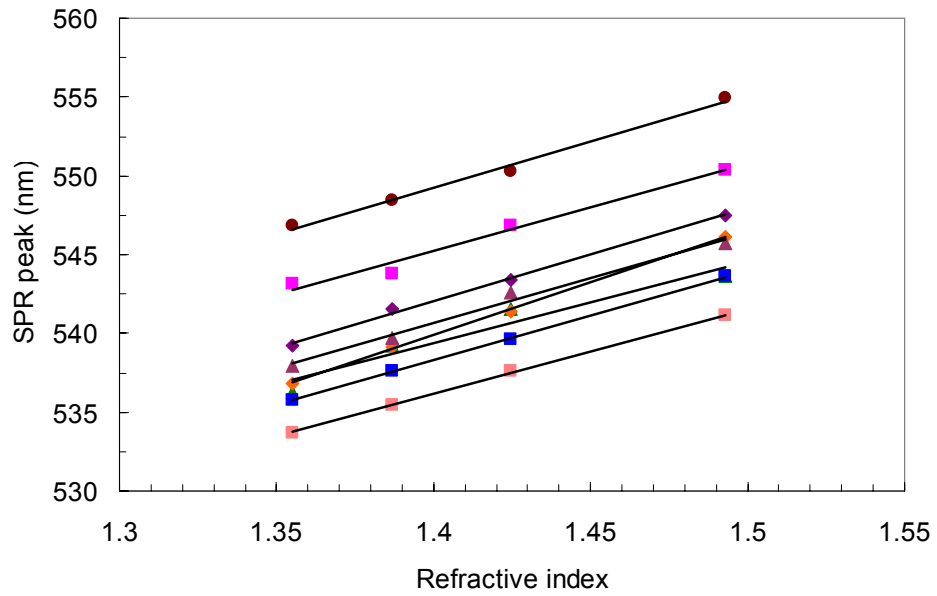


Figure 6: Response functions of gold nanoparticle films immersed in four different liquid solvents. The different data sets correspond to replicate gold films that are different due to variability in the deposition process. The solvents used, in order of refractive index, are acetone, n-heptane, dichloromethane and toluene.

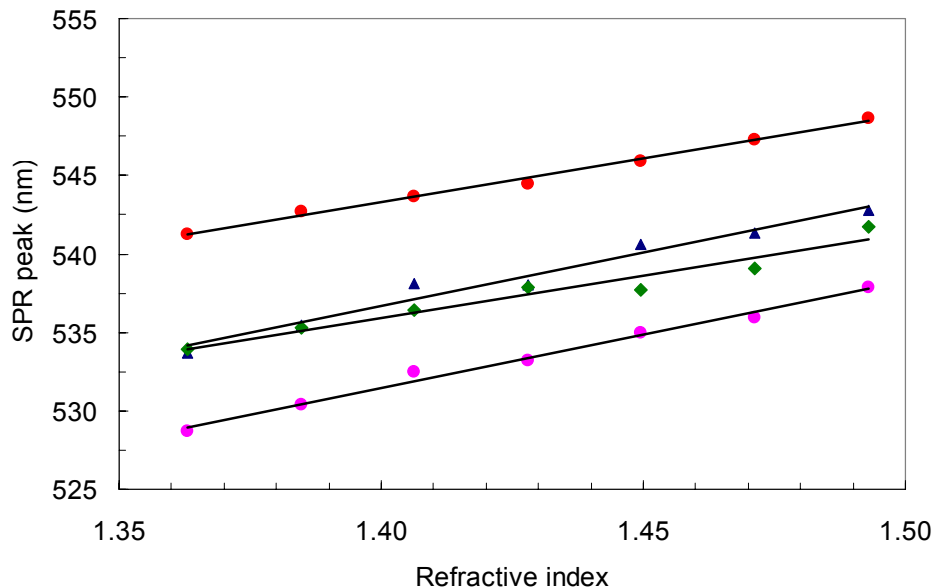


Figure 7: The response functions of gold nanoparticle films determined using an ethanol/toluene binary solvent series. Data for four different gold films are shown. (NOTE: assumes that the refractive index of the mixtures is the composition-weighted average of the refractive indices of toluene and ethanol)

In Figure 8, changes in the SPR peak position as a result of exposure to 2-chloroethyl ethyl sulfide vapour are shown as a function of time. In this experiment, the nanoparticle film was exposed to three distinct partial pressures of 2-chloroethyl ethyl sulfide. The different partial pressures correspond to conditions where the gas bulb was saturated with 2-chloroethyl ethyl sulfide vapour at 23, 35, and 53 °C. Following an initial period of equilibration at ambient conditions, saturated 2-chloroethyl ethyl sulfide vapour was injected into the cell. An instantaneous ~ 0.7 nm increase in peak position was observed as seen in Figure 8. The SPR peak position was then seen to exponentially decay to slightly lower wavelengths over 45 min. After this time, the cell was evacuated and the SPR peak position was seen to rapidly drop, accordingly. A second injection of 2-chloroethyl ethyl sulfide vapour at a higher partial pressure caused a similar jump in the SPR peak position, although to higher wavelengths. A rapid drop to baseline was observed immediately on evacuating the cell a second time and after a period of keeping the cell under vacuum a third injection at a higher partial pressure led to a correspondingly higher shift in the SPR peak position. In all cases, the SPR initially jumped to higher wavelengths when exposed to 2-chloroethyl ethyl sulfide vapour. Subsequently, there was an exponential decay to lower wavelengths, approaching a constant value until the cell was evacuated at which time a step to lower wavelength was observed. Higher partial pressures of 2-chloroethyl ethyl sulfide manifested higher jumps initially and higher wavelength values in the plateau regions prior to evacuation. In Fig. 9, analogous data are shown for a case when the cell and the bath are both at room temperature. The four steps therefore correspond to repeat measurements. The lower graph in Fig. 9 shows the step heights, on the right side of the steps where the cell has equilibrated, compared against themselves. The average value is 534.55 ± 0.02 nm, which indicates that the SPR measurements are reproducible to ± 0.02 nm.

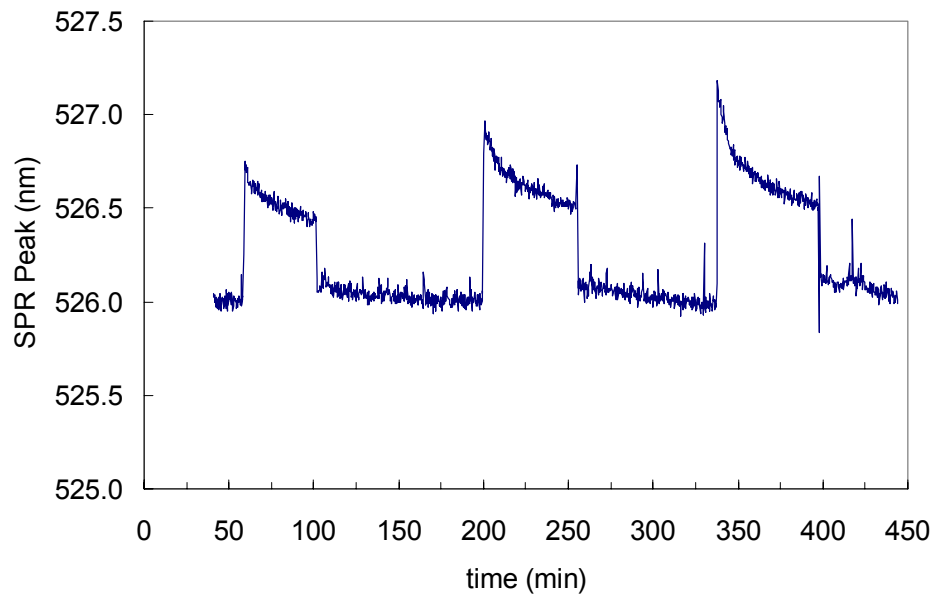


Figure 8: SPR peak position vs. time for an experiment where a gold nanoparticle film was exposed to 2-chloroethyl ethyl sulfide vapour. Each step up in wavelength corresponds to an injection of vapour into the gas cell containing the nanoparticle film. Each step down corresponds to evacuation of the cell. The SPR peak position at each time (10 s) was determined by fitting Eq 1 to the SPR absorbance spectrum. See text for details.

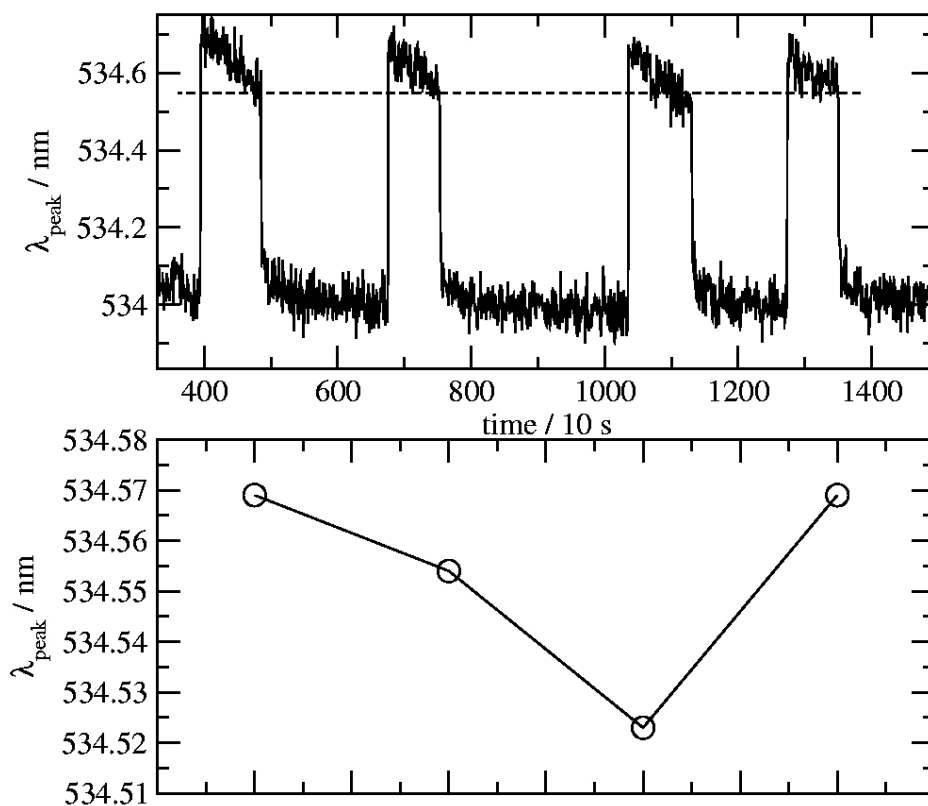


Figure 9: SPR peak position vs. time for an experiment where a gold nanoparticle film was exposed to 2-chloroethyl ethyl sulfide vapour is shown in the upper graph. Each step up in wavelength corresponds to an injection of vapour into the gas cell containing the nanoparticle film. Each step down corresponds to evacuation of the cell. The SPR peak position at each time (10 s) was determined by fitting Eq 1 to the SPR absorbance spectrum. The broken line is a guide to the eye to help show the reproducibility of the step size. Both cell and bath were at room temperature. The lower graph is a plot of the step size, 80 acquisitions after the initial injection, determined for each measurement. See text for details.

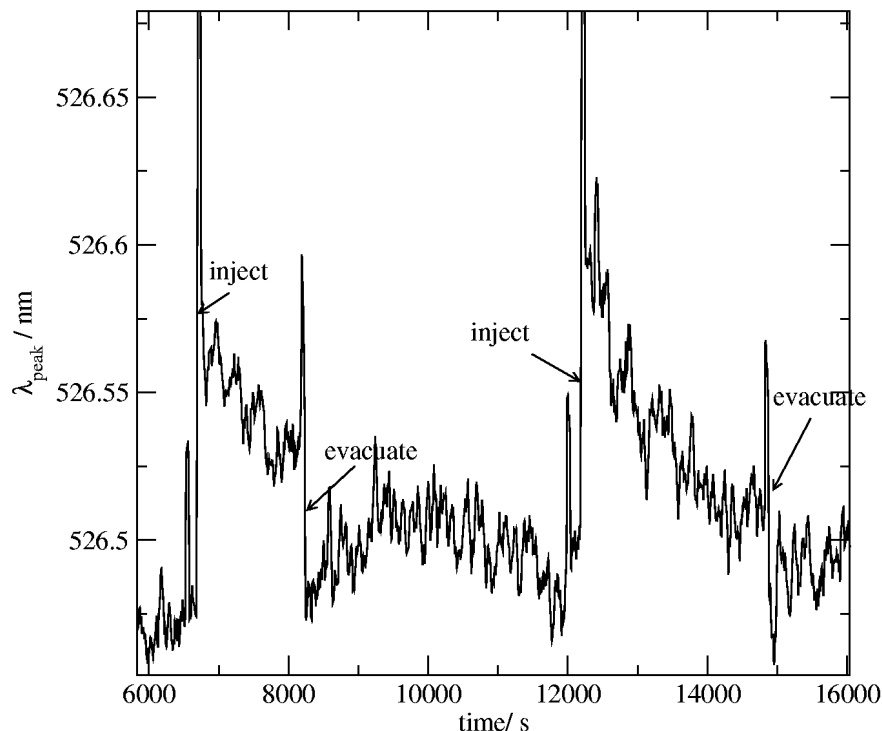


Figure 10: SPR peak position vs. time for an experiment where a gold nanoparticle film was exposed to paraoxon vapour. Each step up in wavelength corresponds to an injection of vapour into the gas cell containing the nanoparticle film. Each step down corresponds to evacuation of the cell. The SPR peak position at each time (10 s) was determined by fitting Eq 1 to the SPR absorbance spectrum. See text for details

In Figure 10, analogous data are shown for paraoxon. As for 2-chloroethyl ethyl sulfide, the different partial pressures correspond to conditions where the gas bulb was saturated with paraoxon vapour at 54 and 73 °C. Comparing Figure 8 and Figure 10, similar behaviour is observed; the SPR peak wavelength is seen to shift to a higher wavelength upon exposure to vapour and return to a baseline value upon evacuation of the cell. However, in Figure 10, the magnitude of the shifts is seen to be much smaller. At room temperature, paraoxon has a vapour pressure five orders of magnitude lower than that of 2-chloroethyl ethyl sulfide (0.00004 mm Hg vs. 2.4 mm Hg respectively). The smaller shift correlates with the smaller amount of vapour injected into the cell. Accordingly, much less paraoxon is adsorbed to the surface of the gold nanoparticles in these experiments. In Figure 11, the data corresponding to a similar experiment conducted with formaldehyde vapour are shown. In sharp contrast to the relatively small shift in the SPR peak position observed for 2-chloroethyl ethyl sulfide and paraoxon vapour, shifts of ~12 nm in the SPR peak position were measured for formaldehyde. Formaldehyde vapour was generated by heating solid paraformaldehyde in the glass bulb to 70 °C. The large shift in the SPR peak position following injection of the formaldehyde vapour into the cell was attributed to the repolymerization of formaldehyde to paraformaldehyde on the surface of the gold nanoparticles as the gas in the cell cooled to room temperature. Evacuating the cell to 10^{-3} Torr overnight failed to return the SPR peak position to its original value. Further heating of the cell to 80 °C, several degrees above the temperature at which the vapour was injected, shifted the SPR peak to a lower wavelength

but again did not completely return it to its original value. An additional period of heating at 250 °C for several hours was required to return the SPR peak to a value of ~525 nm (data not shown).

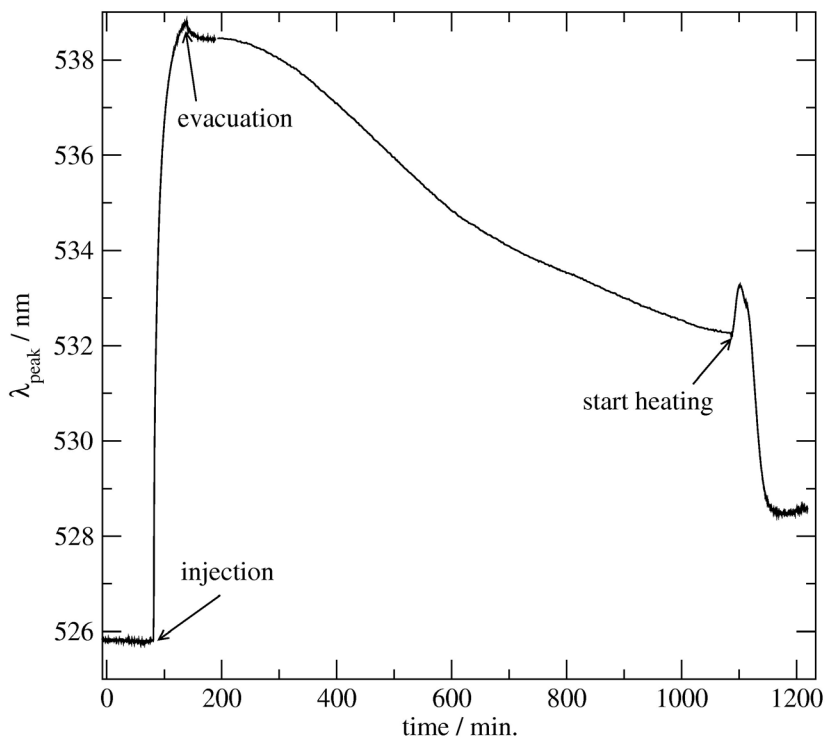


Figure 11: Plot of SPR peak position vs. time collected when a gold nanoparticle film was exposed to formaldehyde. The times corresponding to injection, evacuation, and heating of the gas cell are labelled.

Discussion

The utility of nanoparticle-SPR spectroscopy as a sensor technology suitable for exposure detection depends on many factors affecting sensitivity and stability. The oxidative state (cumulative charge), size, and cleanliness of the nanoparticles are synthesis-related factors that impact sensitivity. Synthesis of Au nanoparticles using the citrate reduction method is a route by which nanoparticles of different sizes can be made depending on the synthesis conditions used. For gold, the size of the particles made is reflected by their colour. The method described above yielded cherry red (CR) solutions a sample spectrum of which is shown in Figure 2. These solutions are stable for months. Such stability indicates a lack of aggregation or coalescence of particles in these solutions, which suggests that the nanoparticles carry a charge (likely negative according to literature).[38] The charge repels particles from each other thus stabilizing the solution. The peak position of the SPR absorption band, found by fitting Eq 1 to the spectrum in Figure 2, is 517.87 nm and is characteristic of relatively small particles.[35,39] To first order, the peak position is related to the size of the nanoparticles by[4]

$$\omega_s = \frac{A v_F}{r} \quad \text{Eq. (4)}$$

where ω_s is frequency (in Hz) corresponding to the SPR peak position, A is a proportionality factor with value assumed to be one, v_F is the Fermi velocity with value of $1.4 \times 10^8 \text{ cm s}^{-1}$ for Au, and r is the radius of the metal particle. Strictly, this formula applies only for a metal particle in vacuum but for a crude estimate of particle size we can use the value of ω_s for our particles in solution. From this formula and the 517.87 nm value obtained from Figure 2, the diameters of the nanoparticles synthesized are in the order of 4.8 nm. This value is in rough agreement with the SPR peak data presented in Figure 3, which suggests a diameter of 14 nm via comparison with literature, and in agreement with the STM imaging data shown in Figure 4 that suggest a diameter of ~ 2.5 nm, as discussed above. Using the traditional definition of nanoparticles as those with diameters between 1 and 100 nm,[29] the particles synthesized are approaching the lower limit and are relatively small. Larger particles have SPR bands shifted to longer wavelengths as illustrated in Figure 3. Here, larger nanoparticles were synthesized by reducing gold onto the surfaces of the cherry red particles, then using these larger particles as seeds onto which more gold was reduced, and so on. The spectra of the different sized particles are shown in Figure 3. The colours of the solutions were cherry red, red wine, and blue corresponding to SPR peak maximums at 520 nm, 543 nm and 558 nm respectively. From the literature, an estimate of the nanoparticle diameter associated with each SPR peak maximum shown in Figure 3 is 14 nm for the SPR at 520 nm, 74 nm for the SPR at 543 nm, and 86 nm for the SPR at 558 nm.[35]

Deposition of nanoparticles onto substrates risks aggregation of the particles, which would adversely affect their sensitivity. It is self-evident that aggregates of nanoparticles would have much of the nanoparticle surface in regions of contact between particles leaving little of the nanoparticle surfaces exposed and available for adsorption of molecular species, which is prerequisite for the resulting shift in the SPR peak position. Significant aggregation is known to cause a red shift in the SPR maximum of sufficient magnitude that the nanoparticles appear blue.[18,40] To the eye, our nanoparticle films made using the silanization/deposition

procedure appear pink in colour. The observed red shift in the plasmon peak position from 517.87 to 523.59 nm is relatively small considering the significant change in the nature of the medium surrounding the particles in going from an aqueous environment to their immobilisation on quartz substrates. The 523.59 nm value was obtained by fitting Eq 1 to the spectrum of quartz-deposited Au nanoparticles shown in Figure 5. The fact that the films synthesized here are not blue indicates that no significant aggregation or multi-layer deposition of the nanoparticles occurred during the deposition process onto the quartz substrates. The films must therefore be near-monolayer in thickness and the nanoparticles must be well dispersed without much direct contact between them. The nanoparticle films are therefore very suitable for sensor applications as the surfaces of most of the nanoparticles are freely exposed and therefore accessible for adsorption of target molecules.

In Figure 6, the SPR peak position associated with quartz-deposited nanoparticle films is plotted as a function of the refractive index of the solvents in which the nanoparticle films have been immersed. Data are shown for eight different nanoparticle films. As seen, all of the slides yield response functions with nearly the same slope. That is, the responsiveness of the films are nearly the same with values of $57.53 \pm 1.62 \text{ nm RIU}^{-1}$ (RIU = refractive index unit). Similar results were obtained using toluene-ethanol binary mixtures as shown in Figure 7. The responsiveness is expected to be sensitive to differences in the nanoparticle films and affected by factors such as nanoparticle aggregation and multi-layer deposition, both of which serve to decrease the amount of nanoparticle surface exposed and available to interact with the surrounding medium. The comparable slopes for the eight different films are an indication, therefore, that the nanoparticle film preparation methodology employed is consistent, yielding very similar films on different days, etc. The data in Figure 6 and Figure 7 also indicate that the responsiveness of the nanoparticle films is high relative to literature examples. By comparison, response functions of triangular silver particles synthesized with the latex-sphere lithography method, limited to particles with dimensions no less than approximately 50 nm, yield slopes of 190 nm RIU^{-1} . [22] At first glance, this responsiveness is more than three times greater than that obtained for our $9 \pm 6 \text{ nm}$ diameter particles. However, if we consider that the surface area of the 50 nm particles is approximately fifty times that of our $9 \pm 6 \text{ nm}$ diameter particles, much less material would have to be adsorbed on the surface of our small diameter nanoparticles to manifest an equivalent change in refractive index and a concomitant shift in the SPR peak position. Accordingly, we expect our nanoparticle films to be as much as fifteen times more sensitive to the presence of adsorbed compounds than the larger Ag particles. The clear advantage of using smaller particles supports use of the solution-phase reduction methods over the nano-sphere lithography method as the films obtained are more sensitive for the former.

The high responsiveness of the nanoparticle films suggests that slight changes in composition of *gas-phase* mixtures may also trigger a SPR response even though the change in the refractive index of the gas medium is very small. To probe the film response to an exposure to gas-phase warfare agent simulants, the films were exposed to varying partial pressures of 2-chloroethyl ethyl sulfide. The 2-chloroethyl ethyl sulfide (which is chemically very similar to sulfur mustard) data are shown in Figure 8. As seen, each injection of 2-chloroethyl ethyl sulfide manifested an increase in the SPR peak position to longer wavelengths. Considering the vapour pressure of 2-chloroethyl ethyl sulfide is relatively low (3.4 Torr at 25 °C), [41] the $\sim 1 \text{ nm}$ jump observed is an indication that relatively small amounts of gas-phase species can be detected with the nanoparticle films. To place the 1 nm value in perspective, with our apparatus shifts in the order of 0.02 nm can be measured, as described above. Accordingly,

species with vapour pressures more than two orders of magnitude lower than that of 2-chloroethyl ethyl sulfide could be detected. The data shown in Figure 8 also illustrate the real-time responsiveness of the nanoparticle films. In less than one spectral acquisition (~10 s) the film responded to the exposure event and a 1 nm shift in the SPR peak position resulted. Similarly, the films responded to evacuation of the cell, and the concurrent removal of 2-chloroethyl ethyl sulfide vapour from the cell, in less than 10 s. The recovery of the gold nanoparticle films to baseline values once the toxic vapours were removed is evidence that binding of the 2-chloroethyl ethyl sulfide is reversible and therefore the film can be cycled through multiple exposure-evacuation cycles and still respond with an observable change in SPR peak position, as seen in Figure 8.

Following exposure to 2-chloroethyl ethyl sulfide, the SPR peak position (λ_{peak}) is seen (Figure 8) to rise sharply and then fall off slightly over a period of minutes. The extent of the decay varies and is more when the injected gas is at higher temperature and is negligible when the temperature of the injected gas is equal to the cell temperature. We can attribute this decay to cooling and the associated drop in partial pressure of 2-chloroethyl ethyl sulfide in the cell. Initially, the gas arrives in the cell at the gas-bulb temperature. The gas then equilibrates to cell temperature. With cooling, the pressure of the gas decreases. For a reversible adsorption reaction $CIEES + M \leftrightarrow CIEES-M$ where M represents the nanoparticle and $CIEES$ represents 2-chloroethyl ethyl sulfide, a decrease in the partial pressure of CIEES will cause desorption of CIEES from the nanoparticle surface and manifest a decrease in λ_{peak} , as observed in Figure 8. To first order, the rate of cooling will follow Newton's rate of cooling law, which has an exponential form compatible with the decays observed in Figure 8. Fits of a generic exponential function to the sections of data where decay is observed yield k values in the order of 0.001 s^{-1} , which is a reasonable value for a cooling rate. A sample fit is shown in Figure 12 and seen to be in agreement with the experimental data. With decreasing temperature difference between the temperature of the injected gas and the cell temperature the rate of cooling is observed to decrease, consistent with Newton's cooling law. Also, the rate is not affected by the cell temperature, specifically. That is, the rate of decay depends on the *difference* between cell and gas temperature, specifically, and not on the temperature of the cell. This observation strongly supports the assignment of the decay observed in Figure 8 and Figure 12 to a gas cooling process, which is an artefact of the experimental approach and not discussed further.

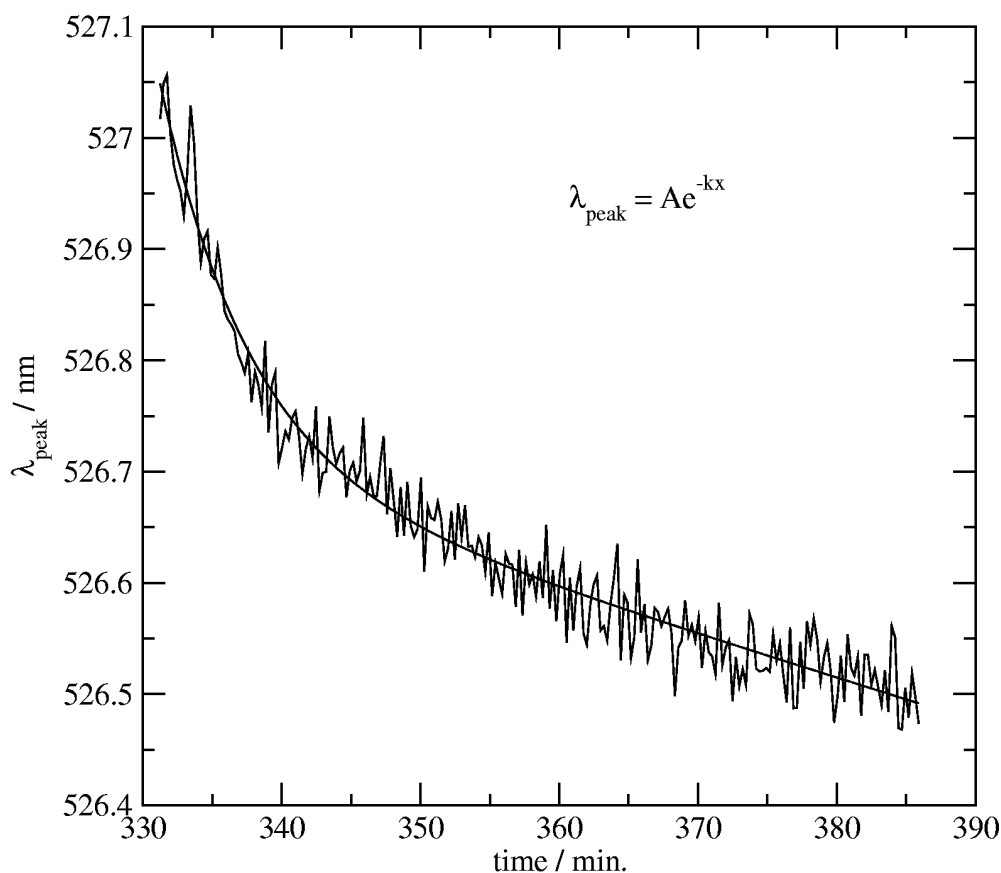


Figure 12: A section of the data shown in Fig. 8 corresponding to the highest temperature, and therefore highest 2-chloroethyl ethyl sulfide pressure, employed. The solid line is a fit of a generic exponential function to the data.

To further quantify the sensitivity of the SPR response, the magnitudes of the shift in SPR peak position ($\Delta\lambda$) observed have been plotted in Figure 13 as a function of the concentration of 2-chloroethyl ethyl sulfide to which the gold nanoparticle film was exposed. Three of the data points (those lying above $\lambda_{peak} = 0.75$ nm) were derived from the data presented previously in Figure 8 and correspond to the change in the value of λ_{peak} that occurred immediately following successive exposure of the gold nanoparticle films to 2-chloroethyl ethyl sulfide vapours, prior to any exponential decays as a result of cooling etc. The fourth data point, showing a λ_{peak} of approximately 0.25 nm, was determined from a separate experiment at a 2-chloroethyl ethyl sulfide concentration of 20 μM . As seen, the 2-chloroethyl ethyl sulfide experiments were conducted under μM concentration conditions. The overall form of the response is distinctly curved as expected. As mentioned above, nanoparticle films are most sensitive to species adsorbed directly to the nanoparticle surface. Accordingly, as seen in Figure 13, at low concentrations $\Delta\lambda$ increases rapidly with increasing concentration while at higher concentrations the rate of increase in $\Delta\lambda$ with increasing concentration is much less. Considering the signal to noise in Figure 8, Figure 10 and Figure 12, we estimate 0.02 nm as near the lower limit of the resolution of our apparatus and data analysis

methodology. This value agrees with the $\pm .02$ nm reproducibility determined above. From Figure 13, a $\Delta\lambda$ of 0.02 corresponds to a 600 pM concentration of 2-chloroethyl ethyl sulfide. Such expressions of sensitivity are molecule-specific as they depend somewhat on the affinity of the gold nanoparticles for the target molecule of interest. In the case of 2-chloroethyl ethyl sulfide, significant adsorption to the nanoparticles is expected as sulfides are well known to bind to gold.[42,43] Such adsorption will manifest a significant change in the effective refractive index near the gold nanoparticles and a corresponding shift in the SPR peak position. Species with little affinity for the particles will not adsorb and much less of a shift in SPR peak position will result.

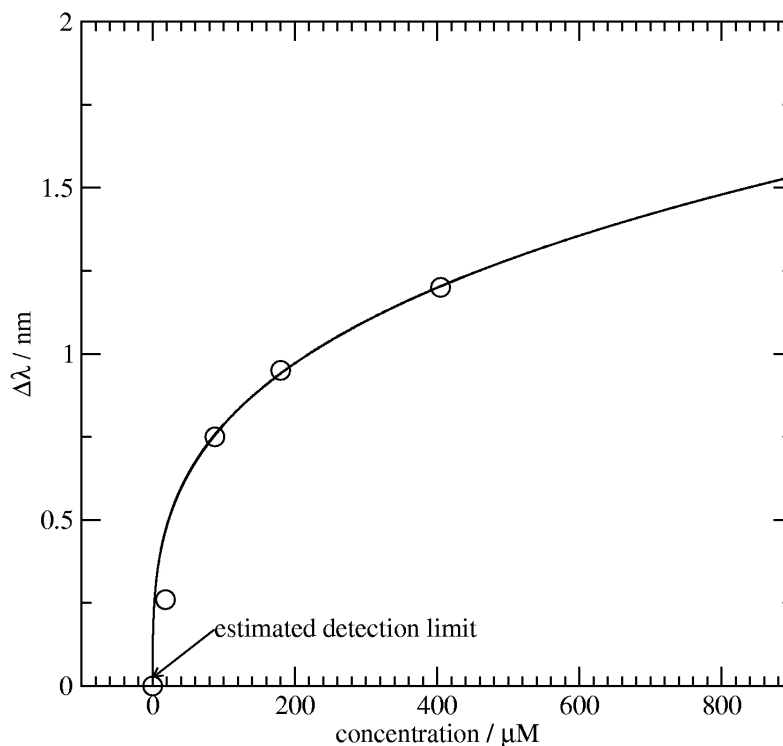


Figure 13: Plot of the change in SPR peak position ($\Delta\lambda$) observed upon exposure of a gold nanoparticle film to 2-chloroethyl ethyl sulfide versus concentration of the sulfide. The solid line is presented as a guide to the eye of the trend in the data.

As a further test of the sensitivity of the gold nanoparticle SPR approach to sensing an exposure-to-toxic-agent event, gold nanoparticle films were exposed to paraoxon. Paraoxon has physical and chemical properties very similar to those of nerve agents. It has a vapour pressure of 7×10^{-5} Torr (1 mg m^{-3}) at 25°C , which is nearly five orders of magnitude lower than that of 2-chloroethyl ethyl sulfide. In fact, the vapour pressure of paraoxon is lower than that of any of the classical nerve agents. The hallucinogen and central nervous system depressant agent BZ (3-quinuclidinyl benzilate) is an exception. Compton lists its vapour pressure as $\sim 0.5 \text{ mg.m}^{-3}$ at 70°C . [44] Data for paraoxon are shown in Figure 10. As seen, distinct jumps in SPR peak position were observed when the nanoparticle film was exposed to paraoxon vapour. That is, the nanoparticle films display a small but discernable response. As

for 2-chloroethyl ethyl sulfide, the response is found to be reversible and λ_{peak} returns to its original value upon evacuation of paraoxon from the gas cell. The concentration of paraoxon in the cell is $\sim 2 \times 10^{-9}$ M. This value approaches the 600 pM value estimated to be the lower detection limit of the gold nanoparticle SPR approach (see above) demonstrating that concentrations of warfare agent simulants near this level can indeed be detected.

In addition to establishing that SPR technology can be used to sense chemical warfare agent simulant exposure events, preliminary tests of the usefulness of this approach to toxic industrial chemical exposure events were also carried out. The most troublesome of the industrial chemicals are those with very high vapour pressures because these are not readily adsorbed by common carbon filter media and therefore the risk of such vapours passing through the filter and exposing the user is high. One of these highly hazardous chemicals is formaldehyde. In Figure 11, the data acquired upon exposure of a gold nanoparticle film to formaldehyde are shown. Indeed, a shift of the SPR peak position to longer wavelengths is observed. Unlike 2-chloroethyl ethyl sulfide and paraoxon, however, the peak position continues to shift to longer wavelengths indefinitely. Before evacuation and removal of the formaldehyde, the peak position had climbed to a value ~ 13 nm greater than the pre-exposure value. A shift of this magnitude is comparable to that observed upon immersion of a nanoparticle film in a liquid as seen in Figure 6 and Figure 7. Postulating that the 13 nm shift observed is the result of formation of a layer of liquid formaldehyde on the gold nanoparticle film is not reasonable considering the very high vapour pressure of formaldehyde. A more likely explanation is that the formaldehyde polymerized, forming para-formaldehyde, on the nanoparticle-film surface. Aldehydes are known to be prone to such polymerization reactions.[45] Consistent with this interpretation, evacuating the gas cell produced no immediate return of the SPR peak position to the pre-exposure value. Instead a slow decrease in SPR peak position was observed which seems to asymptotically approach a value much higher than the pre-exposure one. To return to this value required significant heating as seen in Figure 11, consistent with an endothermic de-polymerization process. Despite the relatively complicated chemistry involved, the experiments clearly show that a significant shift in SPR peak position occurs upon exposure to formaldehyde, a highly hazardous, toxic industrial chemical.

Summary and Conclusions

Gold nanoparticles of 9 ± 6 nm in diameter have been synthesized using the citrate reduction method. These nanoparticles have been successfully deposited onto quartz substrates without inducing any significant aggregation of the particles. The resulting nanoparticle films were found to respond to changes in refractive index of the medium surrounding them in a linear manner. This responsiveness was found to be significantly higher than literature examples of other nanoparticle film responsiveness, which we attribute to the relatively small size of our particles. Exposure of the films to gas-phase formaldehyde was found to manifest a shift in the SPR peak position of ~ 13 nm. This shift is of the magnitude expected upon immersion of the nanoparticle film in a liquid. As this result is incompatible with the gas-phase nature of the experiment, we suggest that polymerization of the formaldehyde, forming para-formaldehyde, is occurring on the gold nanoparticle surface. Regardless, the experiment does establish that formaldehyde, which is on the list of highly hazardous toxic industrial chemicals, is readily detected. The responsiveness of the nanoparticle films upon exposure to 2-chloroethyl ethyl sulfide (simulating sulfur mustard) and paraoxon (simulating nerve agent) has also been investigated. In both cases, a significant shift of the SPR peak position was observed. Analysis of the data establish a lower detection limit of ~ 600 pM and ~ 1 nM for 2-chloroethyl ethyl sulfide and paraoxon, respectively. On the basis of these tests, it is concluded that 2-chloroethyl ethyl sulfide and paraoxon are readily sensed by the gold nanoparticle films using the SPR approach and that this approach offers pM sensitivity.

Annexes

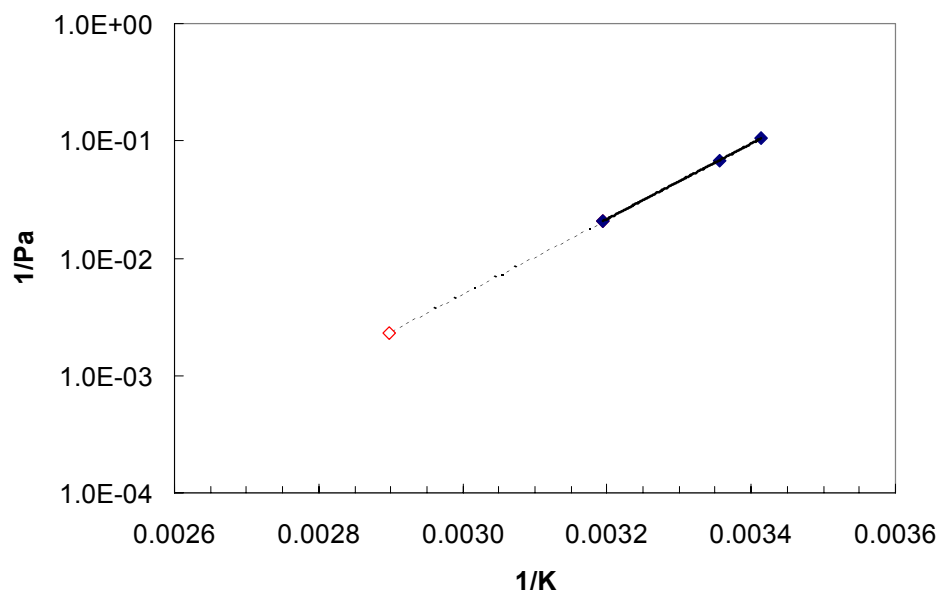
Annex A: Calculation of Saturated Vapour Pressure

Sulphur Mustard						
Pressure (mm Hg)	Pressure (Pa)	1/Pa	Temperature (°C)	Temperature (K)	1/K	Volatility (mg.m ⁻³)
0.072	9.57	0.10447	20	293	0.00341	624.72
0.110	14.62	0.06838	25	298	0.00336	938.42
0.361	48.05	0.02081	40	313	0.00319	2937.44
<i>3.240</i>	<i>430.75</i>	<i>0.00232</i>	72	345	<i>0.00290</i>	<i>23888.39</i>

Note: values in italics are predicted.

Data for 0.072 mm Hg @ 20 °C. Volatility at 40 °C from Compton.[44]

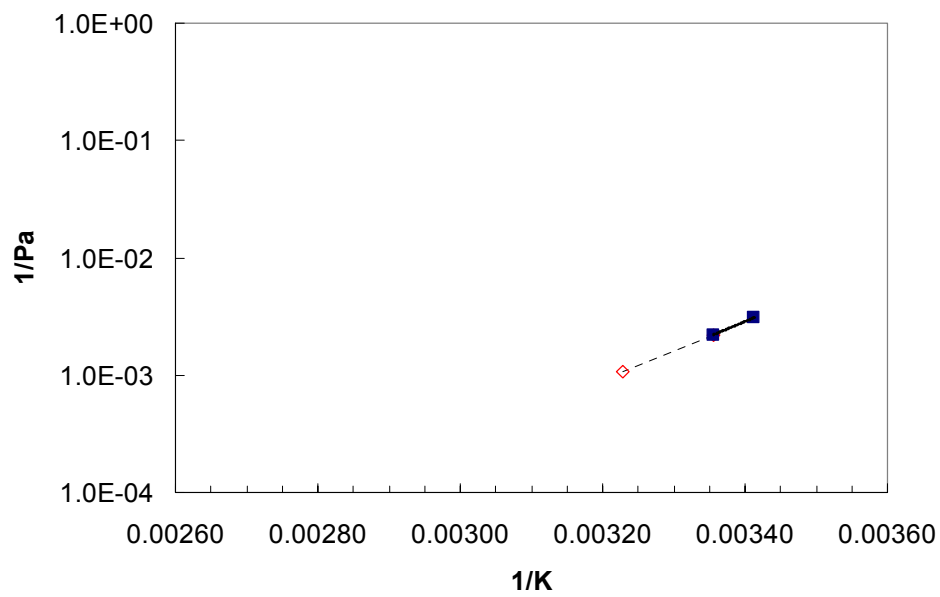
Data for 0.11 mm Hg @ 25 °C.[46]



2-chloroethyl ethyl sulphide						
Pressure (mm Hg)	Pressure (Pa)	1/Pa	Temperature (°C)	Temperature (K)	1/K	Volatility (mg.m ⁻³)
2.436	323.86	0.00309	20	293	0.00341	16600.20
3.400	452.02	0.00221	25	298	0.00336	22739.48
7.114	945.73	<i>0.00106</i>	37	310	<i>0.00323</i>	55220.32

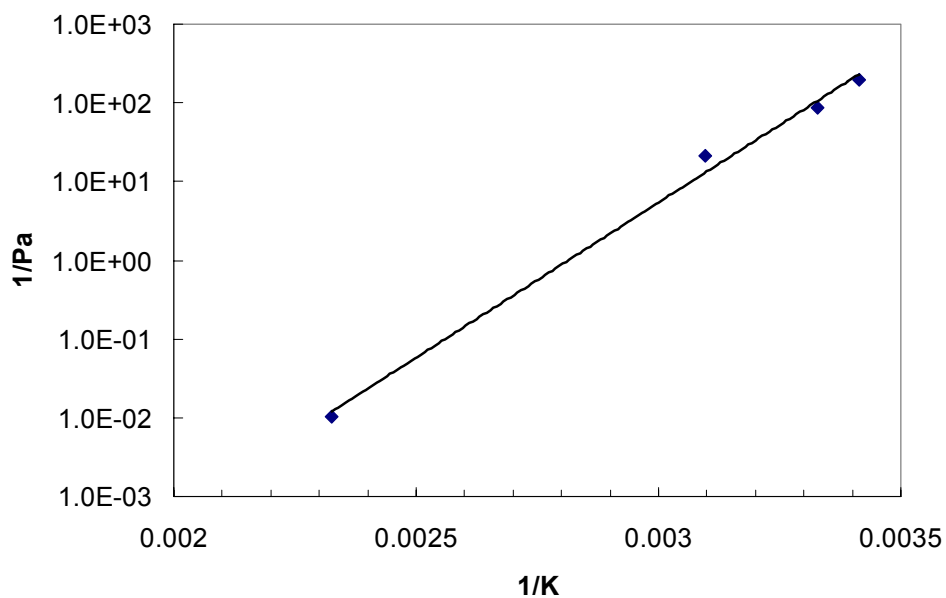
Note: values in italics are predicted.

Data for 3.4 mm Hg @ 25 °C and for volatility 16600 mg.m⁻³ at 20 °C from Bennett et al.[41]



Paraoxon						
Pressure (mm Hg)	Pressure (Pa)	1/Pa	Temperature (°C)	Temperature (K)	1/K	Volatility (mg.m ⁻³)
7.500E-07 (2)	9.971E-05	1.003E+04	0.0	273.0	0.003663	0.05732
3.900E-05 (1)	5.185E-03	1.929E+02	20.0	293.0	0.003413	0.51607
8.600E-05 (3)	1.143E-02	8.746E+01	27.4	300.4	0.003329	1.07923
3.500E-04 (2)	4.653E-02	2.149E+01	50.0	323.0	0.003096	8.30400
7.200E-01 (3)	9.572E+01	1.045E-02	157.0	430.0	0.002326	6765.15

Note: (1) Reifenrath, William G.; Hawkins, George S.; Kurtz, Michael S., J.Pharm.Sci., CODEN: JPMSAE, 80(6), 1991, 526-532; BABS-5588044; (2) 2. Schrader, G., Die Entwicklung neuer insektizider Phosphorsaeure-Ester, 3. Aufl. Weinheim 1963 S. 260; (3) Williams, Ind.Eng.Chem., CODEN: IECHAD, 43, 1951, 950, 952. The previous references supplied by Dr R. Clewley, personal communication.



B

List of symbols/abbreviations/acronyms/initialisms

DND	Department of National Defence
SPR	Surface Plasmon Resonance
UV	ultraviolet
vis	visible
STM	Scanning tunnelling microscope
a. u.	Absorbance units
CR	Cherry red
λ_{peak}	Wavelength of maximum absorbance of a peak in a spectrum
η	Refractive index
m	Responsiveness
v_F	Fermi velocity
ω_s	SPR frequency
r	Radius
RIU	Refractive index unit
$\Delta\lambda$	Change in wavelength

References

- 1 McFarland, A. D.; Van Duyne, R. P. *Nano Letters* **2003**, 3(8), 1057–1062.
- 2 Aslan K.; Zhang J.; Lakowicz J.R.; Geddes C.D. *J. Fluorescence* **2004**, 14(4), 391–400.
- 3 Nath, N.; Chilkoti, A. *J. Fluorescence* **2004**, 14(4), 377–389.
- 4 Alvarez, M.; Khoury, J. T.; Schaaff, G.; Shafigullin, M. N.; Vezmar, I.; Whetten, R. L. *J. Phys. Chem. B* **1997**, 101(19), 3706–3712.
- 5 Jung, L. S.; Campbell, C. T.; Chinowsky, T. M.; Mar, M. N.; Yee, S. S. *Langmuir* **1998**, 14, 5636–5648.
- 6 Creighton, J. A.; Eadon, D. G. *J. Chem. Soc., Faraday Trans.*, **1991**, 87, 3881.
- 7 Knoll, W. *Ann. Rev. Phys. Chem.* **1998**, 49, 569–638.
- 8 Kurihara, K.; Suxuki, K. *Anal. Chem.* **2002**, 74, 696–701.
- 9 Malinsky, M. D.; Kelly, K. L.; Shatz, G. C.; Van Duyne, R. P. *J. Am. Chem. Soc.* **2001**, 123(7), 1471–1482.
- 10 Ekgasit, S.; Thammacharoen, C.; Knoll, W. *Anal. Chem.* **2004**, 76, 561–568.
- 11 Ekgasit, S.; Thammacharoen, C.; Yu, F.; Knoll, W. *Anal. Chem.* **2004**, 76, 2210–2219.
- 12 Taton, T. A.; Mirkin, C. A.; Letsinger, R. L. *Science* **2000**, 289(5485), 1757–1760.
- 13 Mirkin, C. A.; Letsinger, R. L.; Mucic, R. C.; Storhoff, J. J. *Nature* **1996**, 382(6592), 607–609.
- 14 Elghanian, R.; Storhoff, J. J.; Mucic, R. C.; Letsinger, R. L.; Mirkin, C. A. *Science* **1997**, 227(5329), 1078–1080.
- 15 Mucic, R. C.; Storhoff, J. J.; Mirkin, C. A.; Letsinger, R. L. *J. Am. Chem. Soc.* **1998**, 120, 12674–12675.
- 16 Storhoff, J. J.; Elghanian, R.; Mucic, R. C.; Mirkin, C. A.; Letsinger, R. L. *J. Am. Chem. Soc.* **1998**, 120(9), 1959–1964.
- 17 Storhoff, J. J.; Lazarides, A. A.; Mucic, R. C.; Mirkin, C. A.; Letsinger, R. L.; Schatz, G. C. *J. Am. Chem. Soc.* **2000**, 122(19), 4640–4650.
- 18 Lazarides, A. A.; Schatz, G. C. *J. Phys. Chem. B* **2000**, 104(3), 460–467.
- 19 Kelly, K. L.; Lazarides, A. A.; Schatz, G. C. *Computing in Science & Engineering* **2001**, 3(4), 67–73.
- 20 Haes, A. J.; Stuart, D. A.; Nie, S.; Van Duyne, R. P. *J. Fluorescence* **2004**, 14(4), 355–367.
- 21 Nath, N.; Chikoti, A. *J. Fluorescence* **2004**, 14, 377–389.
- 22 A. J. Haes.; R. P. Van Duyne. *J. Am. Chem. Soc.* **2002**, 124, 10596–10604.
- 23 Schatz, G. C.; Van Duyne, R. P. In *Handbook of Vibrational Spectroscopy*; J. M. Chalmers., P. R. Griffiths., Eds.; John Wiley & Sons Ltd, Chichester, **2002**.
- 24 Wurtz, G. A.; Im, J. S.; Gray, S. K.; Wiederrecht, G. P. *J. Phys. Chem. B*, **2003**, 107(51), 14191 – 14198.

-
- 25 Klar, T.; Perner, M.; Grosse, S.; von Plessen, G.; Spirkl, W.; Feldmann, J. *Phys. Rev. Lett.* **1998**, *80*(19), 4249–4252.
- 26 Michaels, A. M.; Nirmal, M.; Brus, L. E. *J. Am. Chem. Soc.* **1999**, *121*(43), 9932–9939.
- 27 Turkevich, J.; Stevenson, P. C.; Hillier, J. *Disc. Faraday Soc.* **1951**, *11*, 55-75.
- 28 Schmid, G. *Chem. Rev.* **1992**, *92*, 1709–1727.
- 29 Murray, C. B.; Kagan, C. R.; Bawendi, M. G. *Annu. Rev. Mater. Sci.* **2000**, *30*, 545–610.
- 30 Hulteen, J. C.; Van Duyne, R. P. *J. Vac. Sci. Technol. A* **1995**, *13*, 1553–1558.
- 31 Hulteen, J. C.; Treichel, D. A.; Smith, M. T.; Duval, M. L.; Jensen, T. R.; Van Duyne, R. P. *J. Phys. Chem. B* **1999**, *103*(19), 3854–3863.
- 32 Ji, X.; Zheng, J.; Xu, J.; Rastogi, V. K.; Cheng, T.-C.; DeFrank, J. J.; Leblanc, R. M.; *J. Phys. Chem. B*, **2005**, *109*(9), 3793-3799.
- 33 Lip, D. *J. Def. Sci.* **2001**, *6*(1), 48-54.
- 34 Wagner, G. W.; Koper, G. B.; Lucas, E.; Decker, S.; Klabunde, K. J.; *J. Phys. Chem. B*, **2000**, *104* (21), 5118-5123.
- 35 Murillo, L. E.; Viera, O.; Vicuna, E.; Briano, J. G.; Castro, M.; Ishikawa, Y.; Irizarry, R.; Sola, L.; *Nanotech* **2002**, *2*, Technical Proceedings of the 2002 International Conference on Computational Nanoscience and Nanotechnology, Chpt 16: Material and Nanostructures Science, “Growth Kinetics of Gold Nanoparticles”
- 36 Mark, G. I.; Biro, L. P.; Gyulai, J. *Phys. Rev. B*, **1998**, *58*(19), 12645-12648.
- 37 Brio, L. P.; Lazarescu, S.; Lambdin, P.; Thiry, P. A.; Fonseca, A.; Nagy, J. B.; Lucas, A. A. *Phys. Rev. B*, **1997**, *56*, 12490.
- 38 Hussain, S.; Youngs, I. J.; Ford, I. J. *J. Phys. D: Appl. Phys.* **2004**, *37*, 318-325.
- 39 Pipino, A. C. R.; Woodward, J. T.; Meuse, C. W.; Silin, V. *J. Chem. Phys.* **2004**, *120*, 1585-1593.
- 40 Lazarides, A. A.; Schatz, G. C.; *J. Chem. Phys.* **2000**, *112*(6), 2987-2993.
- 41 Bennet S. R.; et al. *Environmental Hazards of Chemical Agent Simulants*. Aberdeen Proving Ground, MD. CRDC-TR-84055. (**1984**), 43.
- 42 Troughton, E. B.; Bain, C. B.; Whitesides, G. M.; Allara, D. L.; Porter, M. D. *Langmuir*, **1988**, *4*(2), 365-385.
- 43 Lavrich, D. J.; Wetterer, S. M.; *J. Phys. Chem. B*, **1998**, *102*(18), 3456-3465.
- 44 Compton, A.F. *Military Chemical and Biological Agents: Chemical and toxicological properties*, The Telford Press, Caldwell, NJ, **1987**
- 45 Vogel, A. I. *A Text-Book of Practical Organic Chemistry*, 3rd ed., Longman Group Ltd. London, **1956**, 319.
- 46 Monroe, N. B. et al; *Environ Health Perspect.*, **1999**, *107*, 933-974.

UNCLASSIFIED
SECURITY CLASSIFICATION OF FORM
(highest classification of Title, Abstract, Keywords)

DOCUMENT CONTROL DATA		
(Security classification of title, body of abstract and indexing annotation must be entered when the overall document is classified)		
<p>1. ORIGINATOR (the name and address of the organization preparing the document. Organizations for who the document was prepared, e.g. Establishment sponsoring a contractor's report, or tasking agency, are entered in Section 8.)</p> <p>Defence R&D Canada – Suffield PO Box 4000, Station Main Medicine Hat, AB T1A 8K6</p>	<p>2. SECURITY CLASSIFICATION (overall security classification of the document, including special warning terms if applicable)</p> <p style="text-align: center;">Unclassified</p>	
<p>3. TITLE (the complete document title as indicated on the title page. Its classification should be indicated by the appropriate abbreviation (S, C or U) in parentheses after the title).</p> <p style="text-align: center;">Surface Plasmon Resonance Spectroscopy of Gold Nanoparticle-Coated Substrates: Use as an Indicator of Exposure to Chemical Warfare Simulants (U)</p>		
<p>4. AUTHORS (Last name, first name, middle initial. If military, show rank, e.g. Doe, Maj. John E.)</p> <p style="text-align: center;">Pedersen, Dr. David B. and Duncan, Dr. E.J. Scott</p>		
<p>5. DATE OF PUBLICATION (month and year of publication of document)</p> <p style="text-align: center;">August 2005</p>	<p>6a. NO. OF PAGES (total containing information, include Annexes, Appendices, etc)</p> <p style="text-align: center;">31</p>	<p>6b. NO. OF REFS (total cited in document)</p> <p style="text-align: center;">46</p>
<p>7. DESCRIPTIVE NOTES (the category of the document, e.g. technical report, technical note or memorandum. If appropriate, enter the type of report, e.g. interim, progress, summary, annual or final. Give the inclusive dates when a specific reporting period is covered.)</p> <p style="text-align: center;">Technical Report</p>		
<p>8. SPONSORING ACTIVITY (the name of the department project office or laboratory sponsoring the research and development. Include the address.)</p> <p style="text-align: center;">Defence R&D Canada – Suffield</p>		
<p>9a. PROJECT OR GRANT NO. (If appropriate, the applicable research and development project or grant number under which the document was written. Please specify whether project or grant.)</p>	<p>9b. CONTRACT NO. (If appropriate, the applicable number under which the document was written.)</p>	
<p>10a. ORIGINATOR'S DOCUMENT NUMBER (the official document number by which the document is identified by the originating activity. This number must be unique to this document.)</p> <p style="text-align: center;">DRDC Suffield TR 2005-109</p>	<p>10b. OTHER DOCUMENT NOS. (Any other numbers which may be assigned this document either by the originator or by the sponsor.)</p>	
<p>11. DOCUMENT AVAILABILITY (any limitations on further dissemination of the document, other than those imposed by security classification)</p> <p>(x) Unlimited distribution () Distribution limited to defence departments and defence contractors; further distribution only as approved () Distribution limited to defence departments and Canadian defence contractors; further distribution only as approved () Distribution limited to government departments and agencies; further distribution only as approved () Distribution limited to defence departments; further distribution only as approved () Other (please specify):</p>		
<p>12. DOCUMENT ANNOUNCEMENT (any limitation to the bibliographic announcement of this document. This will normally corresponded to the Document Availability (11). However, where further distribution (beyond the audience specified in 11) is possible, a wider announcement audience may be selected).</p>		

UNCLASSIFIED
SECURITY CLASSIFICATION OF FORM

13. ABSTRACT (a brief and factual summary of the document. It may also appear elsewhere in the body of the document itself. It is highly desirable that the abstract of classified documents be unclassified. Each paragraph of the abstract shall begin with an indication of the security classification of the information in the paragraph (unless the document itself is unclassified) represented as (S), (C) or (U). It is not necessary to include here abstracts in both official languages unless the text is bilingual).

Gold nanoparticles with diameters of 9 ± 6 nm have been synthesized, using the citrate reduction method, and deposited onto quartz substrates. The responsiveness of the resulting gold nanoparticle films to gas-phase warfare agent simulant exposures has been examined using 2-chloroethyl ethyl sulfide and paraoxon. Significant shifts in the peak position of the surface plasmon resonance associated with the nanoparticles were observed in both cases. This shift was reversible and the peak positions returned to their pre-exposure values once the simulants were removed. The response to the exposure events was also found to be faster than ~ 10 s, the rate at which data was acquired in the experiments. A larger shift was observed upon exposure of the films to formaldehyde, a highly hazardous toxic industrial chemical. Unlike, 2-chloroethyl ethyl sulfide and paraoxon, the shift was not readily reversible and extensive heating and pumping under vacuum was required to shift the peak position back to pre-exposure values. Through analysis of the 2-chloroethyl ethyl sulfide and paraoxon data, ~ 600 pM and ~ 2 nM are estimated as lower detection limits for the two simulants, respectively.

14. KEYWORDS, DESCRIPTORS or IDENTIFIERS (technically meaningful terms or short phrases that characterize a document and could be helpful in cataloguing the document. They should be selected so that no security classification is required. Identifiers, such as equipment model designation, trade name, military project code name, geographic location may also be included. If possible keywords should be selected from a published thesaurus, e.g. Thesaurus of Engineering and Scientific Terms (TEST) and that thesaurus-identified. If it is not possible to select indexing terms which are Unclassified, the classification of each should be indicated as with the title.)

CB
Chemical
Biological
Agents
Vapour
Protection
Nanoparticles
Sensor
Gold
Films
Simulants